Fibroblasts from distinct pancreatic pathologies exhibit disease-specific properties

Lawrence N Barrera[1*], **Anthony Evans**[1*], Brian Lane[2], Sarah Brumskill[1], Frances E Oldfield[1], Fiona Campbell[3], Timothy Andrews[3], Zipeng Lu[4], Pedro A Perez-Mancera[1], Triantafillos Liloglou[1], Milton Ashworth[1], Mehdi Jalali[1], Rebecca Dawson[1], Quentin Nunes[1], Phoebe A Phillips[5], John F Timms[6], Christopher Halloran[1], William Greenhalf[1], John P Neoptolemos[7], and Eithne Costello[1]
*** Equal Contribution**

Author affiliations:
[1]Department of Molecular and Clinical Cancer Medicine, University of Liverpool, Liverpool, UK
[2]School of Medical Sciences, Division of Cancer Sciences, University of Manchester, Manchester, UK
[3]Department of Histopathology, Royal Liverpool University Hospital, Liverpool, UK
[4]Pancreas Center, The First Affiliated Hospital with Nanjing Medical University, Nanjing, China
[5]Pancreatic Cancer Translational Research Group, Lowy Cancer Research Centre, School of Medical Sciences, University of New South Wales (UNSW Sydney), Sydney, Australia
[6]Institute for Women's Health, University College London, London, UK
[7]Department of General, Visceral and Transplantation Surgery, University of Heidelberg, Heidelberg, Germany

Running title: Diseased pancreatic fibroblasts retain identity

Correspondence:
Eithne Costello
Institute of Translational Medicine
Department of Clinical Cancer Medicine,
University of Liverpool,
2nd Floor Sherrington Building,
Ashton Street,
Liverpool
L69 3GE
Email: ecostell@liverpool.ac.uk
Telephone: +44 (0)151 795 8032

Disclosure: The authors declare no potential conflicts of interest.

Key words: PDAC; pancreatic stellate cells; cancer-associated fibroblasts; tenascin C; microRNAs.

Abstract

Although fibrotic stroma forms an integral component of pancreatic diseases, whether fibroblasts programmed by different types of pancreatic diseases are phenotypically distinct remains unknown. Here we show that fibroblasts isolated from patients with pancreatic ductal adenocarcinoma (PDAC), chronic pancreatitis (CP), periampullary tumors (PAT), and adjacent normal (NA) tissue (N=34) have distinct mRNA and miRNA profiles. Compared to NA-fibroblasts, PDAC-associated fibroblasts were generally less sensitive to an anti-fibrotic stimulus (NPPB) and more responsive to positive regulators of activation such as TGFβ1 and WNT. Of the disease-associated fibroblasts examined, PDAC- and CP-derived fibroblasts shared greatest similarity, yet PDAC-associated fibroblasts expressed higher levels of Tenascin C (TNC), a finding attributable to miR-137, a novel regulator of TNC. TNC protein and transcript levels were higher in PDAC tissue versus CP tissue and were associated with greater levels of stromal activation, and conditioned media from TNC-depleted PDAC-associated fibroblasts modestly increased both PDAC cell proliferation and PDAC cell migration, indicating that stromal TNC may have inhibitory effects on PDAC cells. Finally, circulating TNC levels were higher in patients with PDAC compared to CP. Our characterization of pancreatic fibroblast programming as disease-specific has consequences for therapeutic targeting and for the manner in which fibroblasts are used in research.

Introduction

The extensive fibrotic stroma associated with pancreatic diseases play an integral role in their pathogenesis. Activated fibroblasts constitute the most significant component of disease-associated desmoplastic stroma (1). Pancreatic stellate cells (PSCs), a major source of pancreatic fibroblasts, are resident lipid-storing cells, which in health are quiescent, and characterized by many lipid droplets rich in vitamin A. Pancreatic injury causes the activation of PSCs to myofibroblast-like cells. This is associated with loss of cytoplasmic lipid droplets, increased proliferation and enhanced expression of α-smooth muscle actin (α-SMA), as well as extracellular matrix (ECM) components (2). Where pancreatic injury is long-lasting e.g. in chronic pancreatitis (CP) or pancreatic ductal adenocarcinoma (PDAC), persistent fibroblast activation leads to overproduction of collagen, fibronectin, laminin and hyaluronic acid resulting in a dense fibrotic meshwork.

In mouse models of pancreatic cancer, PSCs increase tumor growth, promote metastasis, and accompany cancer cells to metastatic sites where they stimulate angiogenesis (3). There is evidence that the dense collagenous meshwork produced by activated fibroblasts physically prevents drug delivery to the tumor cells (4). Moreover, cancer–associated fibroblasts have been reported to scavenge the chemotherapeutic drug gemcitabine, reducing the levels of drug available to tumor cells (5). On the other hand, depleting pancreatic fibroblasts from PDAC tumors in mice yielded aggressive tumors and decreased survival (6,7). Thus, a complex picture emerges of cells with the apparent contradictory capabilities of both protecting against tumor aggression and promoting tumor progression.

Understanding how best to target disease-associated pancreatic fibroblasts is a priority. An early study identified significant overlap in gene expression of desmoplastic stroma from PDAC and the fibrous stroma of CP (8). Consistent with this, isolated activated fibroblasts from either CP or PDAC share morphological and functional characteristics (9). However, whether pancreatic fibroblasts,

activated in the context of different pancreatic diseases or in culture, are similar or whether they are uniquely programmed by their environments remains an unanswered question in the field. Answering this question has important implications for how we therapeutically target these cells in different diseases and for how pancreatic fibroblasts are used in research.

Using a combination of miRNA and mRNA expression profiling of fibroblasts isolated from PDAC, CP, periampullary tumors (PAT) and areas of histologically normal pancreas, followed by comprehensive validation, we show that activated fibroblasts derived from different pancreatic disease types are distinct.

Materials and methods

Pancreatic tissue and blood samples

Resected pancreatic tissue and blood samples were obtained following the approval of the UK Health Research Authority in accordance with the Declaration of Helsinki, including ethical approval (London – South East Research Ethics Committee, Ref: 16/LO/1630) and written informed consent, from patients undergoing pancreatic surgery at the Royal Liverpool University Hospital. For discovery work, activated fibroblasts from areas of diseased pancreas were isolated from patients with pancreatic ductal adenocarcinoma (PDAC, n=6), periampullary tumors (PAT, n=5) comprising ampullary and duodenal tumors, and chronic pancreatitis (CP, n=5). Unmatched adjacent-morphologically normal pancreatic tissue from patients with Mucinous Cystic Neoplasm (n=1), intraductal papillary mucinous neoplasm (IPMN) (n=1), PDAC (n=1) and PAT (n=2) was used to isolate adjacent-normal pancreatic stellate cells (PSCs). For independent validation fibroblasts were isolated in the same manner as the discovery set from an additional 13 patients (PDAC, n=9; CP, n=3 and Normal, n=1). Finally, commercially available human primary normal pancreatic fibroblasts (NF; Vitro

Biopharma) were also analyzed. A portion of each specimen was formalin-fixed and stained with hematoxylin and eosin to confirm the histopathology.

Primary fibroblasts isolation

Diseased fibroblasts (PDAC, CP and PAT) were isolated from pancreatic tissue using the outgrowth method (10) with modifications. Briefly, fibrotic pancreatic tissue, identified following gross analysis of the resected specimen by a pathologist, was collected in ice-cold phosphate-buffered saline containing 1% penicillin-streptomycin. Tissue was cut into 1-2 mm^3 pieces, seeded in a six-well cell culture uncoated plate in the presence of Iscove's Modified Dulbecco's Medium (IMDM) supplemented with 20% FBS, 2% L-glutamine, 1% penicillin-streptomycin and maintained at 37˚C in a humidified atmosphere of 5% CO2/95% air until fibroblasts grew out (two to four weeks to reach 80% confluence). The tissue pieces were removed when fibroblasts reached about 30% confluence. The medium was changed twice weekly, and cells were grown to 80% confluence, harvested and stored in liquid nitrogen.

Unmatched adjacent-morphologically normal pancreatic tissue was used to isolate adjacent-normal pancreatic stellate cells (PSCs) using the density gradient method (11). Isolated quiescent PSCs were cultured in a six-well cell culture uncoated plate (and thus culture-activated) until cells reached 80% (two to four weeks) to achieve adequate yield and purity as previously described by Sherman et al (12) and are hereafter referred to as normal activated (NA). These cells were cultured in IMDM supplemented with 20% FBS, 2% L-glutamine, 1% penicillin-streptomycin and maintained at 37˚C in a humidified atmosphere of 5% CO2/95% air. The medium was changed twice weekly, and cells were grown to 80% confluence, harvested and stored in liquid nitrogen.

The commercially available normal fibroblasts (NF) were grown using commercial low serum medium (NF-LSM) (MSC-GRO, Vitro Biopharma) and IMDM supplemented with 10% FBS, 2% L-glutamine, 1% penicillin-streptomycin (NF-HSM) using the same conditions detailed above.

For mRNA / miRNA array experiments, diseased fibroblasts, normal activated fibroblasts (NA), and commercially available normal fibroblasts (NF) from early passages (P1 or P2) were recovered from liquid nitrogen simultaneously and placed in a T75 flask with IMDM supplemented with 10% FBS, 2% L-glutamine, 1% penicillin-streptomycin. The media was replenished twice weekly and cells were grown to 80% confluence before RNA was isolated as described below.

Cell lines

Human PDAC cell lines, MIAPaca-2, Panc-1 and HeLa were obtained from the American Type Culture Collection. Cells were validated by STR profiling and tested for mycoplasma using e-Myco plus mycoplasma PCR detection kit (iNTRON Biotechnology) following manufacturer instructions.

Microarray experiments

Total RNA isolated from the fibroblasts obtained was hybridized onto GeneChip Affymetrix miRNA 4.0 and Human Transcriptome Array 2.0 Affymetrix. The labelling, hybridization, scanning, and data extraction of mRNA and miRNA array experiments were performed at the Centre for Genomic Research, University of Liverpool.

Human Transcriptome Array

50ng of total RNA (free from DNA) was labelled using the Ovation Pico WTA system V2 (NuGen Technologies, Inc.). This kit prepares amplified cDNA for gene expression analysis. Following second strand synthesis the cDNA was purified using Agencourt RNAClean XP beads prior to SPIA amplification. The SPIA amplified cDNA was purified using the Qiagen QIAquick PCR Purification system. Utilizing the Encore Biotin Module 5µg of amplified cDNA was fragmented and Biotin-

labelled before hybridization on Affymetrix GeneChip Human Transcriptome 2.0 arrays (HTA_2.0) (Affymetrix, Inc.). Arrays were hybridized for 17 hours at 45˚C and 60rpm in an Affymetrix GeneChip hybridisation oven 645. Following hybridization the arrays were washed and stained on an Affymetrix GeneChip Fluidics Station 450 using a FS450_0001 script and scanned in an Affymetrix Genechip Scanner 3000G.

microRNA array

130ng of total RNA (free from DNA) was labelled using the FlashTag Biotin HSR RNA Labeling Kit (Affymetrix). This process began with a brief tailing reaction followed by ligation of the biotinylated signal molecule to the target RNA sample. Biotin-labelled samples and controls were added to a hybridization mix and hybridized to Affymetrix GeneChip miRNA 4.0 arrays for 18 hours at 48˚C and 60rpm in an Affymetrix GeneChip hybridization oven 645. Following hybridization, the arrays were washed and stained on an Affymetrix GeneChip Fluidics Station 450 using a FS450_0002 script and scanned in an Affymetrix Genechip Scanner 3000G.

Conditioned media experiments using PDAC cell lines

PANC-1 and MIAPaCa-2 cells were seeded at a density of 7.5×10^5 cells per 75-cm^2 flasks using DMEM + GlutaMAX supplemented with 10% FBS and 1% penicillin-streptomycin. After 24h media was replaced and cells were grown for an additional 72h at which point cells had reached 80-90% confluence. Conditioned media (CM) was collected and filtered using a 0.22µm filter and stored at -80˚C until use. Flasks without cells were processed similarly, as controls. Fibroblasts were seeded in 6-well plates at 8.0×10^4 cells per well using DMEM + GlutaMAX, supplemented with 10% FBS, 1% penicillin-streptomycin and after reaching ~70% confluence cells were incubated with CM diluted 1:2 with fresh DMEM for 48h before RNA was extracted for qRT-PCR analysis.

NPPB treatment

R2796 and R2797 (NA fibroblasts) in addition to R2910 and R3104 (PDAC-associated fibroblasts) were seeded on a 24-well plate at 3.0×10^4 cells per well using DMEM + GlutaMAX supplemented with 10% FBS and 1% penicillin-streptomycin. The next day, cells were washed with PBS twice and further incubated in DMEM + GlutaMAX serum free media supplemented with 1% penicillin-streptomycin whilst being treated with 100nmol/L of human NPPB (Bachem, Switzerland) and water (control) 3 times a day for 48h. This dosing protocol was followed to maintain active levels of NPPB in culture (13).

TGFβ1 treatment

R2796 and R2797 (NA fibroblasts) in addition to R2910, R3104 and R2875 (PDAC-associated fibroblasts) were seeded on a 24-well plate at 3.0×10^4 cells per well using DMEM + GlutaMAX supplemented with 10% FBS and 1% penicillin-streptomycin. The next day cells were washed with PBS twice and further incubated in DMEM + GlutaMAX serum free media supplemented with 1% penicillin-streptomycin whilst being treated with 5ng/ml or 10ng/ml of human TGFβ1 (Millipore) and water (control) for 24h and/or 48h.

Wnt pathway activation

Wnt pathway stimulation was achieved using an L-Wnt-3A cell line (14). In order to generate L-Wnt-3A conditioned media (CM) 1×10^6 cells per T75 flask were seeded using DMEM + GlutaMAX, 10% FBS, 1% geneticin. After 24 hours media was replaced and cells were grown for an additional 72h at which point cells had reached 80-90% confluence. Then, CM was collected and filtered using a 0.22μm filter. In addition, a flask without cells was also filled with culture medium for 72h to generate control media and processed as before. R2796, R2797 and R2951 (NA fibroblasts) in

addition to R3008 and R3072 (PDAC-associated fibroblasts) and R3030 and R334 (PAT-associated fibroblasts) were seeded at 50,000 cells on a 6-well plate for 24h before media was replaced with L-Wnt-3A CM for an additional 24h before RNA was extracted to measure AXIN2 levels using qRT-PCR.

TNC knockdown and collection of conditioned media

Immortalized PDAC-associated and normal activated fibroblasts were seeded on a 6-well plate at 6 × 10^4 cells per well in DMEM + GlutaMAX supplemented with 10% FBS without antibiotics. After 24h cells were transfected using Opti-MEM I reduced serum media followed by addition of Lipofectamine (ThermoFisher Scientific) according to manufacturer's instructions. Two different siRNAs targeting TNC (ON-TARGET plus siRNA Human TNC: #J-009298-07-0005 and #J-009298-05-0005) or a non-targeting control (ON-TARGET plus control pool: #D-001810-10-20) (Dharmacon) with a final siRNA concentration of 30nM were used. The day after the transfection medium was replaced by serum-free media (DMEM + GlutaMAX without antibiotics). Cells were then grown for a further 48h to reach 80-90% confluence. Conditioned media (CM) was collected and filtered using a 0.22µm filter and stored at -80˚C until use for cell migration and proliferation experiments. In addition, cells were lysed to obtain protein.

Migration assays

Transwell cell migration assays were performed using 8µm pore size ThinCertTM cell culture inserts (greiner bio-one) in a 24-well format. MIA PaCa-2 cells were preincubated in serum-free DMEM + GlutaMAX media overnight. 100 µl of cell suspension containing 6 × 104 cells were placed in the insert. The outer chamber was filled with 500µl of conditioned media from the fibroblasts TNC knockdown experiment including controls (diluted 1:2 with DMEM + GlutaMAX and supplemented with 2% FBS) and cells were allowed to migrate for 24h. After incubation, non-migrating cells were

removed from the top of the membrane with cotton swab. Migrated cells were fixed with 70% ethanol and stained with 0.3% crystal violet. Quantification of migration was performed using QuPath (version 0.2.0-m2) (15). Images were taking using a Nikon Eclipse E600 at 4x. The area of migrated cells (crystal violet) and cell-free area were quantified using the pixel classifier tool (applying the Random Trees classifier and using a downsample resolution between 4 and 8). Cell migration of treated cells was expressed as a percentage of control.

Proliferation assays

MIA PaCa-2 cells were plated on a 96-well plate at 5×10^3 cells per well using DMEM + GlutaMAX supplemented with 10% FBS. The following day cells were washed twice with PBS and treated with conditioned media from the normal or PDAC-associated fibroblasts TNC knockdown experiment including controls (diluted 1:2 with DMEM + GlutaMAX and supplemented with 2% FBS). After 48h, cell proliferation was measure using the EZ4U assay system (Biomedica) and a Multiskan FC microplate reader (ThermoFisher Scientific) according to manufacturer's instructions.

microRNA mimics

Immortalized PDAC-associated fibroblasts were seeded on a 24-well plate at 2.0×10^4 cells per well using DMEM + GlutaMAX supplemented with 10% FBS without antibiotics. After 24h miRNA mimics including hsa-miR-137 and hsa-miR-212-3p (30nM) (Qiagen) or AllStars off-target control (30nM) (Qiagen) were diluted in Opti-MEM I reduced serum media (ThermoFisher Scientific) followed by addition of HiPerFect (Qiagen) transfection reagent according to manufacturer's instructions. Complexes were added drop-wise onto the cells and incubated for 48h before RNA or condition media was extracted for qRT-PCR and immunoblotting respectively.

Tissue microarray (TMA) construction

Formalin-fixed paraffin-embedded (FFPE) PDAC and CP specimens were obtained from the Royal Liverpool University Hospital. Matched haematoxylin and eosin stained slides were marked by a specialist histopathologist (FC) for areas of tumor and fibrosis in the PDAC and CP cases respectively. Two TMAs were constructed from PDAC specimens, PDAC TMA #1 (n=41) and PDAC TMA #2 (n=48), with three 0.6mm cores extracted per patient. One TMA was constructed from CP specimens (n=47), with four 0.6mm cores extracted for each patient.

Serum biomarker analysis by multiplex and enzyme-linked immunosorbent assay (ELISA) analysis

A discovery cohort of serum samples were obtained from patients undergoing pancreatic surgery at the Royal Liverpool University Hospital (termed UoL, n=65) and healthy donors (n=15). The discovery cohort was subjected to multiplex quantification of 101 cancer-associated proteins (Human OncologyMAP® v1.0, Myriad Rules-Based Medicine).

ELISAs for TNC (Large FNIII-B, IBL international) were performed according to the manufacturer's instructions and assessed for reproducibility in the UoL discovery cohort (n=75). Upon confirmation, TNC concentrations were determined in an independent cohort of UoL samples (n=155).

Statistical Analysis

All statistical test were performed using R software V.3.5.2. Continues variables were expressed as mean±SEM and compared using a one-way ANOVA or Kruskal Wallis Test, paired or unpaired t-test and Mann-Whitney U test as appropriate; categorical variables were compared using the chi-squared test. Results were considered significant at $p < 0.05$.

Supplemental Methods are described in Supplementary Material and Methods

Results

Disease-associated fibroblasts from pancreatic pathologies show distinct gene expression profiles

To determine the extent to which fibroblasts are programmed by their distinct disease environments we isolated pancreatic fibroblasts and analyzed uniquely low passage (P1 or P2) from a total of 34 individuals, enabling us to compare PDAC, PAT, CP and adjacent normal-derived cells (Figure 1A and Supplementary Table 1). Consistent with others, we found that disease-associated fibroblasts exhibited myofibroblast-like morphology with characteristic expression of α-SMA, desmin, vimentin (Figure 1B) and other common markers of fibroblasts (Supplementary Figure 1A). One day post-isolation, primary normal PSCs contained characteristic lipid droplets as measured by Oil Red O (Figure 1B), however, following expansion in culture, they became activated, gaining expression of α-SMA, and are hereafter called normal activated (NA). None of the isolated cells expressed macrophage (CD68) or epithelial (pan-cytokeratin and EPCAM) (Figure 1B and Supplementary Figure 1A) markers. *KRAS* mutational status was successfully determined for 33 isolates. One isolate, from a PDAC tumor, was found to be heterozygous for mutant *KRAS (G12R)* and was excluded from the study.

mRNA and miRNA gene expression profiles of isolated fibroblasts, as well as commercially available normal fibroblasts (NF) grown in low or high serum, were generated. qRT-PCR analysis of eight randomly selected genes was undertaken to validate our microarray profiling experiments. The expression patterns observed in array data for four mRNAs (Supplementary Figure 1B) and two miRNAs (Supplementary Figure 1C) were confirmed by qRT-PCR in the discovery samples, and for a further two mRNA candidates (Supplementary Figure 1D) in analyses which included independent primary fibroblasts (Independent set, Supplementary Table 1).

Principal component analysis (PCA) of both mRNA (Figure 1C) and miRNA (Figure 1D) expression showed evidence of clustering based on the disease group from which fibroblasts were derived, indicating differences in the nature of activated fibroblasts between disease types.

To explore this further, we compared the extent to which fibroblasts programmed by different pancreatic diseases differ from normal activated fibroblasts. We found 1,469 genes differentially expressed between PDAC-associated fibroblasts and NA, compared to only 776 genes differentially expressed between PAT-associated fibroblasts and NA. This suggested that distinct malignancies program fibroblasts differently. CP fell between PDAC and PAT with 925 differentially expressed genes compared to NA (Figure 1E). Surprisingly, only 24% of genes were commonly dysregulated across the three different diseases compared to NA (Figure 1E), although this rose to 48.5% when the disease-associated fibroblasts groups were compared to NF (Supplementary Figure 2A).

Almost one third (32.2%) of genes significantly altered between PDAC and NA were unique to this comparison group while only 6.6% and 7.3% respectively were exclusive for the CP versus NA and PAT versus NA comparisons (Figure 1E). Interestingly, PDAC and CP shared over 41.5% of genes dysregulated when compared to NA, indicating similarities in the programming of fibroblasts by these disease types.

Consistent with recent reports (16-18), the most enriched canonical pathways associated with disease-associated fibroblasts compared to NA were phagosome maturation, autophagy and endocytosis signaling (Figure 1F). The most common biological functions differentially regulated between disease-associated fibroblasts and NA or NF corresponded to cell movement and migration with key upstream regulators such as TNF, TP53 and TGFβ1 (19-21) altered in these comparison groups (Supplementary Figure 2B, 2C).

Only five miRNAs were significantly dysregulated between PDAC-associated fibroblasts and NA (Supplementary Figure 2D). Similarly, five miRNAs were altered between CP and NA, and four of these were also dysregulated between PDAC-associated fibroblasts and NA. Fibroblasts programmed by PAT had two dysregulated miRNAs compared to NA, one of which was unique to PAT (hsa-miR-92a-1-5p), and the other, hsa-miR-138-1-3p, was also dysregulated in CP and PDAC. Nine miRNAs were dysregulated in all three-disease types compared to NF (Supplementary Figure 2E).

Taken together, our data indicate that while there is commonality between fibroblasts cultured from different pancreatic disease types or normal tissue, the groups are distinct. Given that our PCA analysis showed NA to be more closely related to the other primary fibroblast isolates than the commercially available NF were, we focused subsequent analyses on NA.

PDAC-associated fibroblasts are less responsive to an anti-fibrotic stimulus and more responsive to positive regulators of fibroblast activation than normal activated fibroblasts

Next we sought to understand how PDAC-associated fibroblasts differed from all other disease-associated or NA fibroblasts. Our analysis (Figure 2A) revealed 224 differentially regulated genes between PDAC and PAT-derived fibroblasts and 90 differentially regulated genes between PDAC and CP. Twelve genes were uniquely dysregulated in PDAC-associated fibroblasts compared to all other groups. One of these, NPPB, also known as brain natriuretic peptide was amongst the most highly up-regulated transcripts between groups in both discovery (Figure 2B), and validation samples (Supplementary Figure 2F). Analysis of data from the Gene Expression Omnibus database (Figure 2C, https://www.ncbi.nlm.nih.gov/geo/geo2r/, GEO accession: GSE21440) (22) corroborated our observation. NPPB mRNA levels in fibroblasts derived from PDAC (CAF, n=9) were higher than from control fibroblast lines (HPNE and NF1-3) and from an IPMN (SC-2) (22).

We postulated that the high levels of NPPB in PDAC-associated fibroblasts were the result of *in vivo* tumor-stroma paracrine signaling prior to fibroblast isolation. Indeed, stimulating primary PDAC-derived fibroblasts with conditioned medium from PANC-1 or MIAPaCa-2 cells led to increased NPPB transcription in the fibroblasts (Figure 2D). By contrast, NPPB expression was undetectable in two independent isolates of NA fibroblasts, and consistently remained undetectable after treatment with conditioned medium from pancreatic cancer cell lines. This suggested differences in the ways in which PDAC- and NA-fibroblasts respond to external stimuli. Curiously, for one of the most highly regulated molecules in PDAC-associated fibroblasts, NPPB's function may relate to reducing fibrosis. NPPB is reported to have anti-fibrotic properties in the heart (13) and kidney (23) and inhibits liver fibrosis by preventing activation of hepatic fibroblasts (24). We examined whether incubation of activated pancreatic fibroblasts with NPPB could reverse their activation, leading to diminished α-SMA gene (ACTA2) expression. To avoid bias, we selected NA and PDAC-associated fibroblasts respectively with high (R2796 and R2910) and low (R2797 and R3104) pre-treatment α-SMA levels (Figure 2E). Treatment of fibroblasts with recombinant NPPB protein led to a decrease in α-SMA expression in both NA and PDAC high and low α-SMA expressers (Figure 2F), although the greatest anti-fibrotic effects were observed in NA.

We next evaluated positive regulators of fibroblast activation. Consistent with its prominent role in pancreatic fibrosis (25), Ingenuity Pathway Core Analysis identified TGFβ1 among the top three activated upstream regulators in pancreatic disease-associated fibroblasts compared to NA (Figure 2G, left panel). Treatment of high (R2796 and R2910) and low (R2797, R3104, R2875) α-SMA expressing fibroblasts with TGFβ1 increased the activation state, as measured by α-SMA expression, in both PDAC- and NA-associated fibroblasts (Figure 2G, right panel), with a significant induction of α-SMA observed in PDAC-derived fibroblasts. The canonical Wnt pathway mediates fibroblast activation through interaction with TGFβ (26). The molecular activity predictor tool in IPA predicted that the Wnt pathway was activated in PDAC-associated fibroblasts compared to NA (Figure 2H). To

evaluate Wnt signaling, we incubated NA, PDAC-associated fibroblasts and PAT-associated fibroblasts with conditioned medium from a cell line that constitutively secretes Wnt-3A (14). The resulting induction of AXIN2 expression was observed in both NA and the cancer-associated fibroblasts, with the highest induction seen in cancer-associated fibroblasts (Figure 2I). Collectively, our data on NPPB, TGFβ and WNT signaling demonstrate that fibroblasts activated *in vitro* by the culture process (NA) are functionally distinct from fibroblasts programmed *in vivo* by cancer. PDAC-associated fibroblasts were less readily inactivated than NA, and considerably more responsive to a positive trigger of activation.

Disease-associated fibroblasts from distinct pancreatic disorders exhibit subtype-specific genetic profiles

We next narrowed our focus to fibroblasts programmed by pancreatic diseases, examining differences between fibroblasts from PDAC, CP and PAT (Figure 3A). The greatest overlap in gene expression was between PDAC and CP with only 90 differentially expressed genes. By contrast, PDAC and PAT differed by 224 genes and there were 272 genes differentially regulated between PAT and CP. Interestingly, the most enriched pathway identified by IPA, the *Hepatic Stellate Cell Activation Pathway* was not significantly differentially enriched between PDAC and CP, indicating commonality between the activation of fibroblasts in these two disease types (Figure 3B and 3C). By contrast, this pathway was significantly up-regulated in PDAC compared to PAT, and downregulated in PAT compared to CP (Figure 3B and 3C), highlighting differences in the way in which PAT fibroblasts are activated compared to both PDAC and CP. Gene expression alterations in this pathway can be attributed to upstream regulators such as TGFβ1, p38 MAPK, MAPK and HIF1A, (27,28) which were significantly modulated between these comparison groups (Supplementary Table 2). Four of the top eight pathways identified by IPA were immune-related (Figure 3B). Of note, the genes most commonly dysregulated in these pathways belonged to the major histocompatibility complex (MHC) class I, namely HLA-A, HLA-B, HLA-C, which were downregulated in PDAC-versus-CP and in PDAC-

versus-PAT (Figure 3D). In addition, the *Cell Cycle Control of Chromosomal Replication* and the *ATM Signaling* pathways, which showed no differences between PDAC and CP (Figure 3B) were significantly dysregulated in PAT compared to CP (Figure 3E and 3F).

Taken together, these data indicate significant differences in the pathways activated in disease-associated pancreatic fibroblasts from different pathologies.

Tenascin C levels are elevated in PDAC-associated fibroblasts compared to CP- associated fibroblasts

While this study was ongoing, in parallel research we sought differences in serum proteins from patients with CP and PDAC using a multiplex quantification of 101 cancer-associated proteins (Myriad Rules-Based Medicine's Human OncologyMAP® v1.0 platform). Apart from the well-established carbohydrate antigen tumor markers, CA19-9 and CA125, only circulating Tenascin C (TNC) was significantly upregulated in PDAC compared to CP patients in discovery analysis (Figure 4A) and in an independent validation cohort (Figure 4B, Supplementary Table 3). We considered this finding highly significant, as circulating proteins capable of distinguishing CP from PDAC are extremely rare. Moreover, TNC is not widely expressed in adults, except in the extracellular matrix of diseased or injured tissues. Our serum data drove us to question whether TNC expression was more pronounced in fibroblasts isolated from PDAC than CP. Although not identified as significantly differentially expressed using the stringent criteria of our array analysis, our array data nonetheless indicated lower TNC in CP than in PDAC (Figure 4C). Moreover, RT-PCR confirmed that TNC transcripts were significantly upregulated in PDAC-associated fibroblasts compared to CP-associated fibroblasts (Figure 4D). Immunohistochemistry for TNC in resected PDAC and CP specimens was performed using the same antibody we used in our serum analysis (clone 4C8MS, TNC-FN III-B) and revealed heterogeneous TNC staining, with TNC protein variously present in areas of stroma, benign ducts and tumor cells. Notably, regions of strong staining were observed in the desmoplastic stroma

of tumors even when neighboring epithelia lacked expression (Figure 4E). Tissue microarrays (TMAs) from PDAC and CP cases (Supplementary Table 4) revealed more frequent TNC protein in the stromal compartments of PDAC cases compared to CP cases (60.4% compared with 13.9%, respectively, Figure 4F). TNC-null mice exhibit attenuation of skin and lung fibrosis (29), and TNC has recently emerged as a key regulator of CAFs as part of a Twist1-Prrx1-TNC feedback loop that operates as an ON/OFF switch regulating fibroblast activation (30). We measured the ratio of α-smooth muscle actin (α-SMA) to collagen, defined as the activated stroma index (31) (Figure 4G). PDAC cases with TNC^+ stroma had significantly greater activated stroma index values than those lacking stromal TNC (Figure 4H). RNA *in situ* hybridization for TNC mRNA showed that of 79 PDAC cases examined, 82.3% contained TNC mRNA-expressing cells in the stroma, compared to 47.2% of CP cases (n=36; Figure 4I and J). Together, our data indicate that fibroblasts programmed in the context of CP are distinct from those programmed in the context of PDAC, and this is exemplified by the lower expression of TNC in CP-associated fibroblasts than PDAC fibroblasts.

Depletion of TNC in PDAC-associated fibroblasts promotes migration of cancer cells

We next sought to understand the functional significance, for PDAC cells, of high TNC expression in PDAC-associated fibroblasts (Figure 5A, 5B and 5C). We found that conditioned media from TNC-depleted CAFs but not TNC-depleted NA fibroblasts (Figure 5D) caused significantly greater migration of MIA PaCa-2 cells when compared to conditioned media from control siRNA-treated fibroblasts. Additionally, we found a modest 8% increase in MIA PaCa-2 cell proliferation following exposure to conditioned media from TNC-depleted CAF but not TNC-depleted NA fibroblasts (Figure 5E). Our data indicate that CAF-derived TNC decreases the migration of PDAC cells and has a minor negative effect on PDAC cell growth.

Finally, given that TGFβ1 was one of the top activated upstream regulators in pancreatic disease-associated fibroblasts compared to NA (Figure 2G), along with the well-established function of TGFβ in several key steps of tumorigenesis (32), we questioned whether TNC levels in pancreatic

fibroblasts influenced TGFβ1 levels. We found that TNC depletion in CAF (Figure 5F) but not NA (Figure 5G) was accompanied by significant reduction in TGFβ1 expression. Taken together, our data support the notion that TNC deficiency in CAFs promotes migration of cancer cells, and that this is associated with a parallel reduction in TGFβ1 expression.

miR-137 regulates TNC expression

To explore mechanisms underlying the difference in expression of TNC in PDAC-associated stroma compared to CP stroma, an *in silico* analysis was performed to identify miRNAs with the potential to target the 3' untranslated region (UTR) of TNC mRNA using http://www.miRNA.org. Of 24 candidate miRNAs, two, miR-212-3p and miR-137, tended towards downregulation in PDAC compared to CP (Figure 6A and 6B), the inverse of the observed TNC mRNA levels in PDAC and CP (Figure 4C and 4D). One potential binding site in the UTR of TNC mRNA was identified for hsa-miR-212-3p and two sites were identified for hsa-miR-137 and ranked by mirSVR scoring (Figure 6C). To test whether these microRNAs regulated the expression of TNC, PDAC-associated fibroblasts were treated with mimics of the selected candidate miRNAs. Transfection of a miR-137 mimic but not a miR-212-3p mimic significantly reduced TNC expression levels, at both the mRNA (Figure 6D) and protein level (Figure 6E). A luciferase reporter assay utilizing the TNC 3' UTR binding site for miR-137 with the best mirSVR score value (position 444; mirSVR -1.2304), confirmed that miR-137 targets this region (Figure 6F). Notably, the decrease of luciferase activity was abolished when the TNC 3' UTR target site was mutated. Our data point towards miRNA-mediated fine-tuning of pancreatic fibroblast gene expression contributing to distinct fibroblasts programing between CP and PDAC.

To determine whether TGFβ1 controls the miR-137-TNC axis, we treated CAF and NA with TGFβ1 and measured the expression of both TNC and miR-137. We observed a significant increase in TNC expression in both CAF and NA following TGFβ1 treatment (Figure 6G). Moreover in NA, TGFβ1 treatment was accompanied by significant down-regulation in the expression of miR-137 (Figure 6H), demonstrating that TGFβ can control this axis. Down-regulation of miR-137 was not observed in

CAFs following treatment by TGFβ1. Thus it would appear that other factors may also underpin the regulation of this axis.

Discussion

In the present study, we show the first direct comparison of pancreatic fibroblasts isolated from distinct pancreatic diseases, we provide evidence that pancreatic fibroblasts are programmed by their unique disease-specific environments and that their distinct gene expression persists following isolation. The challenges associated with isolating and characterizing human primary pancreatic fibroblasts has led to this fundamental question remaining unanswered until now. Although all of the disease-associated fibroblasts compared in our study exhibited myofibroblast-like morphology and expressed characteristic markers of activation, less than one quarter of differentially expressed genes were commonly shared between disease groups, compared to NA. When comparisons were restricted to disease-associated fibroblasts only, less than one percent of differentially expressed genes were commonly altered across disease types. This argues against a single common phenotype of pancreatic fibroblast activation and emphasizes the importance of using appropriate fibroblasts to address disease-specific research questions. Similarly, all of the primary fibroblasts isolated for this study, including NA, were subjected to culture, prior to RNA extraction for gene profiling. Whilst one might expect this to have a 'normalizing' effect, isolated fibroblasts exhibited distinct characteristics of the disease group to which they belonged. Notably, NA were more responsive than PDAC-associated fibroblasts to the anti-fibrotic effects of NPPB, (13,23,24) showing large reductions of the fibroblast activation marker α-SMA. Similarly, tumor fibroblasts responded with greater intensity than NA to the activation stimuli of TGFβ and WNT signaling.

The global impact of microRNA regulation in quiescent versus activated pancreatic stellate cells has thus far been performed in rats only (33). Our comparison of primary human NA fibroblasts with human disease-activated fibroblasts revealed only a small proportion of differentially expressed

miRNAs, with no difference found between PDAC and CP or PDAC and PAT. This reflects a tight regulation of miRNAs across pancreatic disease fibroblasts in contrast to the high number of mRNA transcripts differentially regulated.

The activation of PAT-associated fibroblasts was distinctly different from that of PDAC-associated fibroblasts as indicated by the up-regulation of genes associated with the *Hepatic Stellate Cell Activation Pathway* in PDAC-associated fibroblasts compared to PAT- but not CP-associated fibroblasts. Ampullary and duodenal cancer-associated fibroblasts are hardly characterized and warrant further study. Overlap observed between PDAC- and CP-associated fibroblasts may reflect the fact that both diseases can present concurrently, and that fibroblasts in the context of PDAC are educated by both the tumor and by CP. Nonetheless there were significant differences between PDAC- and CP-derived fibroblasts, as exemplified by TNC. The higher TNC transcript and protein levels in PDAC-derived fibroblasts and PDAC resected specimens compared to CP and the positive link between TNC and activated stroma suggests enhanced fibroblast activation in PDAC versus CP in our study.

The consequences, however, of high fibroblast levels of TNC on cancer cell behavior has hardly been examined to date. Our finding that conditioned medium derived from TNC-depleted PDAC-associated fibroblasts enhanced the motility of Mia PaCa-2 cells is intriguing, and implies that the high levels of TNC in PDAC-associated fibroblasts may serve to repel tumoral cells. Consistent with this, TNC knock-out in breast carcinomas allowed the attraction of macrophages (34).

Uncovering miR-137 as a regulator of TNC in disease-associated fibroblasts provides a potential candidate for targeting TNC. Previous studies have reported down-regulation of miR-137 in pancreatic cancer tissues compared to their normal counterpart with its overexpression leading to inhibition of cancer cell invasion and promotion of senescence (35,36). In a study of acute lung

injury, TNC-null lung fibroblasts exhibited impaired responsiveness to TGFβ (37). Our findings that TNC depletion diminishes TGFβ1 expression in pancreatic CAF while TGFβ1 stimulation of CAFs and NA increased TNC expression evidences the important interplay between TNC and TGFβ1 in pancreatic fibrosis. Finally, the identification of TNC as a biomarker with potential to distinguish PDAC from CP warrants further investigation as such circulating biomarkers are lacking.

In conclusion, we present evidence that *in vivo* programming of human fibroblasts is disease-specific and is, at least to an important extent, maintained in culture. Single cell technologies have helped elucidate how stromal CAFs contribute to proliferative and invasive transcriptional programs of PDAC cells, with CAF-secreted TGFβ identified as a key mediator of PDAC cell heterogeneity (38). Moreover, the heterogeneity of human PDAC-associated fibroblasts themselves has been described, with CAFs exhibiting myofibroblast (myCAF), inflammatory (iCAF) or antigen presenting (apCAF) phenotypes (39,40). Future work addressing specific subpopulations of pancreatic fibroblasts from different pancreatic diseases are now required. The prevailing perception that activated pancreatic fibroblasts are a uniform entity that can be used interchangeably in research requires revision. Furthermore, the development of treatments should take into consideration disease-specific features of activated pancreatic fibroblasts.

Acknowledgments: This work was funded by the Pancreatic Cancer Research Fund to E.C, Rosetrees Trust to E.C and L.N.B (M384-F1), Pancreatic Cancer UK to E.C, L.N.B and A.E (2011_Grant-Costello/Timms and RIF2014_03_Costello), the National Institute for Health Research Liverpool Pancreas Biomedical Research Unit to E.C, North West Cancer Research, UK to E.C (CR1142) and Cancer Research UK to E.C. Researchers at UCL were supported by the NIHR University College London Hospitals (UCLH) Biomedical Research Centre to J.F.T. The authors would like to thank Dr Lucille Rainbow at the Centre for Genomic Research for her assistance with microarray preparation,

Dr Nicholas Harper for providing essential reagents and help with the luciferase reporter construct, Mr Luke Taylor and Mr Ben Crosby for their help in searching medical records. We would also like to thank Ms Katie Bullock, Dr Amelia Acha-Sagredo, Mr Luke Wilkinson, Ms Roberta Sanna, Dr Neal Rimmer, Ms Elizabeth Garner and Dr Katharine Hand for excellent technical assistance.

References:

1. Evans A, Costello E. The role of inflammatory cells in fostering pancreatic cancer cell growth and invasion. Front Physiol **2012**;3:270
2. Pang TCY, Wilson JS, Apte MV. Pancreatic stellate cells: what's new? Curr Opin Gastroenterol **2017**;33:366-73
3. Xu Z, Vonlaufen A, Phillips PA, Fiala-Beer E, Zhang X, Yang L*, et al.* Role of pancreatic stellate cells in pancreatic cancer metastasis. Am J Pathol **2010**;177:2585-96
4. Kalluri R. The biology and function of fibroblasts in cancer. Nat Rev Cancer **2016**;16:582-98
5. Hessmann E, Patzak MS, Klein L, Chen N, Kari V, Ramu I*, et al.* Fibroblast drug scavenging increases intratumoural gemcitabine accumulation in murine pancreas cancer. Gut **2018**;67:497-507
6. Rhim AD, Oberstein PE, Thomas DH, Mirek ET, Palermo CF, Sastra SA*, et al.* Stromal elements act to restrain, rather than support, pancreatic ductal adenocarcinoma. Cancer cell **2014**;25:735-47
7. Ozdemir BC, Pentcheva-Hoang T, Carstens JL, Zheng X, Wu CC, Simpson TR*, et al.* Depletion of carcinoma-associated fibroblasts and fibrosis induces immunosuppression and accelerates pancreas cancer with reduced survival. Cancer cell **2014**;25:719-34
8. Binkley CE, Zhang L, Greenson JK, Giordano TJ, Kuick R, Misek D*, et al.* The molecular basis of pancreatic fibrosis: common stromal gene expression in chronic pancreatitis and pancreatic adenocarcinoma. Pancreas **2004**;29:254-63
9. Erkan M, Weis N, Pan Z, Schwager C, Samkharadze T, Jiang X*, et al.* Organ-, inflammation- and cancer specific transcriptional fingerprints of pancreatic and hepatic stellate cells. Mol Cancer **2010**;9:88
10. Bachem MG, Schneider E, Gross H, Weidenbach H, Schmid RM, Menke a*, et al.* Identification, culture, and characterization of pancreatic stellate cells in rats and humans. Gastroenterology **1998**;115:421-32
11. Vonlaufen A, Phillips PA, Yang L, Xu Z, Fiala-Beer E, Zhang X*, et al.* Isolation of quiescent human pancreatic stellate cells: a promising in vitro tool for studies of human pancreatic stellate cell biology. Pancreatology **2010**;10:434-43
12. Sherman MH, Yu RT, Engle DD, Ding N, Atkins AR, Tiriac H*, et al.* Vitamin D receptor-mediated stromal reprogramming suppresses pancreatitis and enhances pancreatic cancer therapy. Cell **2014**;159:80-93
13. Kapoun AM, Liang F, O'Young G, Damm DL, Quon D, White RT*, et al.* B-type natriuretic peptide exerts broad functional opposition to transforming growth factor-beta in primary human cardiac fibroblasts: fibrosis, myofibroblast conversion, proliferation, and inflammation. Circ Res **2004**;94:453-61
14. Willert K, Brown JD, Danenberg E, Duncan AW, Weissman IL, Reya T*, et al.* Wnt proteins are lipid-modified and can act as stem cell growth factors. Nature **2003**;423:448-52
15. Bankhead P, Loughrey MB, Fernandez JA, Dombrowski Y, McArt DG, Dunne PD*, et al.* QuPath: Open source software for digital pathology image analysis. Sci Rep **2017**;7:16878

16. Endo S, Nakata K, Ohuchida K, Takesue S, Nakayama H, Abe T*, et al.* Autophagy Is Required for Activation of Pancreatic Stellate Cells, Associated With Pancreatic Cancer Progression and Promotes Growth of Pancreatic Tumors in Mice. Gastroenterology **2017**;152:1492-506 e24
17. Bi Y, Mukhopadhyay D, Drinane M, Ji B, Li X, Cao S*, et al.* Endocytosis of collagen by hepatic stellate cells regulates extracellular matrix dynamics. Am J Physiol Cell Physiol **2014**;307:C622-33
18. Bauer AS, Nazarov PV, Giese NA, Beghelli S, Heller A, Greenhalf W*, et al.* Transcriptional variations in the wider peritumoral tissue environment of pancreatic cancer. Int J Cancer **2018**;142:1010-21
19. Egberts JH, Cloosters V, Noack A, Schniewind B, Thon L, Klose S*, et al.* Anti-tumor necrosis factor therapy inhibits pancreatic tumor growth and metastasis. Cancer Res **2008**;68:1443-50
20. Arandkar S, Furth N, Elisha Y, Nataraj NB, van der Kuip H, Yarden Y*, et al.* Altered p53 functionality in cancer-associated fibroblasts contributes to their cancer-supporting features. Proc Natl Acad Sci U S A **2018**;115:6410-5
21. Bhowmick NA, Chytil A, Plieth D, Gorska AE, Dumont N, Shappell S*, et al.* TGF-beta signaling in fibroblasts modulates the oncogenic potential of adjacent epithelia. Science **2004**;303:848-51
22. Walter K, Omura N, Hong SM, Griffith M, Vincent A, Borges M*, et al.* Overexpression of smoothened activates the sonic hedgehog signaling pathway in pancreatic cancer-associated fibroblasts. Clin Cancer Res **2010**;16:1781-9
23. Suganami T, Mukoyama M, Sugawara A, Mori K, Nagae T, Kasahara M*, et al.* Overexpression of brain natriuretic peptide in mice ameliorates immune-mediated renal injury. J Am Soc Nephrol **2001**;12:2652-63
24. Sonoyama T, Tamura N, Miyashita K, Park K, Oyamada N, Taura D*, et al.* Inhibition of hepatic damage and liver fibrosis by brain natriuretic peptide. FEBS Lett **2009**;583:2067-70
25. Vogelmann R, Ruf D, Wagner M, Adler G, Menke A. Effects of fibrogenic mediators on the development of pancreatic fibrosis in a TGF-beta1 transgenic mouse model. Am J Physiol Gastrointest Liver Physiol **2001**;280:G164-72
26. Akhmetshina A, Palumbo K, Dees C, Bergmann C, Venalis P, Zerr P*, et al.* Activation of canonical Wnt signalling is required for TGF-beta-mediated fibrosis. Nat Commun **2012**;3:735
27. Tsukada S, Westwick JK, Ikejima K, Sato N, Rippe RA. SMAD and p38 MAPK signaling pathways independently regulate alpha1(I) collagen gene expression in unstimulated and transforming growth factor-beta-stimulated hepatic stellate cells. J Biol Chem **2005**;280:10055-64
28. Wang Y, Huang Y, Guan F, Xiao Y, Deng J, Chen H*, et al.* Hypoxia-inducible factor-1alpha and MAPK co-regulate activation of hepatic stellate cells upon hypoxia stimulation. PLoS One **2013**;8:e74051
29. Bhattacharyya S, Wang W, Morales-Nebreda L, Feng G, Wu M, Zhou X*, et al.* Tenascin-C drives persistence of organ fibrosis. Nat Commun **2016**;7:11703
30. Yeo SY, Lee KW, Shin D, An S, Cho KH, Kim SH. A positive feedback loop bi-stably activates fibroblasts. Nat Commun **2018**;9:3016
31. Erkan M, Michalski CW, Rieder S, Reiser-Erkan C, Abiatari I, Kolb A*, et al.* The activated stroma index is a novel and independent prognostic marker in pancreatic ductal adenocarcinoma. Clin Gastroenterol Hepatol **2008**;6:1155-61
32. David CJ, Massague J. Contextual determinants of TGFbeta action in development, immunity and cancer. Nat Rev Mol Cell Biol **2018**;19:419-35

33. Masamune A, Nakano E, Hamada S, Takikawa T, Yoshida N, Shimosegawa T. Alteration of the microRNA expression profile during the activation of pancreatic stellate cells. Scand J Gastroenterol **2014**;49:323-31
34. Talts JF, Wirl G, Dictor M, Muller WJ, Fassler R. Tenascin-C modulates tumor stroma and monocyte/macrophage recruitment but not tumor growth or metastasis in a mouse strain with spontaneous mammary cancer. J Cell Sci **1999**;112 (Pt 12):1855-64
35. Neault M, Mallette FA, Richard S. miR-137 Modulates a Tumor Suppressor Network-Inducing Senescence in Pancreatic Cancer Cells. Cell Rep **2016**;14:1966-78
36. Xiao J, Peng F, Yu C, Wang M, Li X, Li Z*, et al.* microRNA-137 modulates pancreatic cancer cells tumor growth, invasion and sensitivity to chemotherapy. Int J Clin Exp Pathol **2014**;7:7442-50
37. Carey WA, Taylor GD, Dean WB, Bristow JD. Tenascin-C deficiency attenuates TGF-β-mediated fibrosis following murine lung injury. Am J Physiol Lung Cell Mol Physiol **2010**;299:L785-93
38. Ligorio M, Sil S, Malagon-Lopez J, Nieman LT, Misale S, Di Pilato M*, et al.* Stromal Microenvironment Shapes the Intratumoral Architecture of Pancreatic Cancer. Cell **2019**;178:160-75 e27
39. Elyada E, Bolisetty M, Laise P, Flynn WF, Courtois ET, Burkhart RA*, et al.* Cross-Species Single-Cell Analysis of Pancreatic Ductal Adenocarcinoma Reveals Antigen-Presenting Cancer-Associated Fibroblasts. Cancer Discov **2019**;9:1102-23
40. Ohlund D, Handly-Santana A, Biffi G, Elyada E, Almeida AS, Ponz-Sarvise M*, et al.* Distinct populations of inflammatory fibroblasts and myofibroblasts in pancreatic cancer. J Exp Med **2017**;214:579-96

Figure Legends:

Figure 1. Isolation, characterization and clustering by gene expression profiling of pancreatic fibroblasts. **(A)** Schematic showing fibroblast isolates from different pancreatic diseases using the outgrowth (top) or from unmatched normal appearing tissue using the density gradient methods (bottom) including the total number of isolates per fibroblast type (discovery set plus independent set). **(B)** Representative images of primary PDAC-associated fibroblasts confirming expression of α-SMA, desmin and vimentin. Fibroblasts did not express CD68 or cytokeratin (Scale bar=50μm). In addition, image shows a primary normal PSC containing lipid droplets visible by oil-red O staining one day after isolation. **(C and D)** Principal component analysis with 25,195 gene transcripts (**C**) and 6,631 microRNA genes (**D**) separated samples into 5 subsets. Each sphere (PDAC=6, CP=5, PAT=5 and NA=5) represents one primary sample. Commercial primary normal fibroblasts (NF) cultured with high serum medium (HSM) or low serum medium (LSM) were analyzed in triplicate. **(E)** Venn diagram depicting the number of differentially expressed genes (mRNA array) between disease-associated fibroblasts from PDAC, CP and PAT versus NA fibroblasts, including the number of genes up- or down-regulated per contrast (the percentage is indicated in the parenthesis) **(F)** Top canonical pathways enrichment analysis of differentially expressed genes in all disease-associated fibroblasts versus NA fibroblasts, performed using Ingenuity Pathway Analysis. Fisher's exact test was used to determine *P*-values, with significance set at p=0.05 which translates to –log (P value) of 1.3.

Figure 2. PDAC-associated fibroblasts display greater resistance to the anti-fibrotic effects of NPPB and greater responsiveness to TGFβ1 and WNT signaling compared to NA. **(A)** Venn diagram depicting the number of differentially expressed genes (mRNA array) between PDAC-associated fibroblasts and the other groups. The twelve genes dysregulated between PDAC and all other groups are named, with NPPB highlighted in red as the most up-regulated gene in the list. **(B)** NPPB mRNA array expression measured as Robust Multi-array Average (RMA) in discovery fibroblast isolates (PDAC=6, CP=5 and PAT=5) and normal PSC culture-activated as described in material and methods (NA=5). **(C)** NPPB mRNA expression values from Gene Chips data in pancreatic ductal adenocarcinoma- (CAF), chronic pancreatitis- (NF1-3), pancreatic IPMN tumor- (SC-2) and normal pancreas immortalized-associated fibroblasts (HPNE). Data collected from GEO database accession numbers: GSM535920 to GSM535931 **(D)** qRT-PCR analysis of NPPB expression levels in PDAC-associated fibroblasts (PDAC-F: R2928 and R2875) and NA-associated fibroblasts (NA-F: R2796 and R2797) following incubation for 48 hours with conditioned media from PANC-1 and MIA PaCa-2 cells. Expression was normalized to GAPDH using unconditioned DMEM as control. Data are shown as mean ±SEM; n=3 independent experiments; *P*-value determined by one-way ANOVA with post-hoc Dunnett's test. n.d.= non-detectable expression **(E)** qRT-PCR analysis of ACTA2 expression levels in discovery and independent fibroblast samples. Two PDAC- (R2910 and R3104) and two NA-associated fibroblasts (R2796 and R2797) isolates are highlighted and analyzed in **(F)** by qRT-PCR for ACTA2 after incubation with recombinant human NPPB for 48 hours. Expression levels were compared to control (DMEM) and normalized to GAPDH. Error bars depict mean ±SEM of technical replicates from two NA- and two PDAC-associated fibroblast isolates. *P*-value determined by unpaired t-test using DMEM as control. **(G)** The top 5 upstream regulators (with their predicted activation state) significantly enriched in all disease-associated fibroblasts versus NA fibroblasts, as determined using IPA **(left panel)**. qRT-PCR for ACTA2 after incubation with recombinant human TGFβ1 for 24 hours. Expression levels were compared to control (DMEM) and normalized to GAPDH. Error bars depict mean ± SEM of technical replicates from two NA- (R2796 and R2797) and three PDAC-associated fibroblast isolates (R2910, R3104 and R2875). *P*-value determined by unpaired t-test (**right panel)**. (**H**) Network analysis employing the IPA molecular activity prediction tool to assess directionality of changes in the Wnt signaling pathway for differentially expressed genes in all disease-associated fibroblasts versus NA fibroblasts. **(I)** qRT-PCR analysis of AXIN2 expression levels following incubation with CM from L-Wnt-3A mouse fibroblast cell line for 24 hours. Expression

levels were compared to unconditioned media as control (DMEM) and normalized to GAPDH. Error bars depict mean ± SEM of technical replicates from three NA- (NA-F: R2796, R2797 and R2951), two PDAC- (PDAC-F: R3008 and R3072) and two PAT-associated fibroblasts (PAT-F: R3030 and R3334). *P*-values determined by unpaired t-test.

Figure 3. Diseased pancreatic fibroblasts retain identity *ex vivo*. **(A)** Venn diagram depicting the number of differentially expressed genes (mRNA array) between disease-associated fibroblast groups including the number of genes up- or down-regulated per contrast (the percentage is indicated in the parenthesis) **(B)** Top canonical pathway enrichment analysis of differentially expressed genes between disease-associated fibroblast groups using IPA comparison analysis. Fisher's exact test was used to determine *P*-values, with the dashed line indicating $p<0.05$. **(C-F)** Fold change of gene expression in selected pathways for contrasts analyzed in **B**.

Figure 4. High levels of TNC identified in primary PDAC- compared to CP- associated fibroblasts reflect levels present in tissue and blood. **(A)** Serum levels of TNC in the discovery cohort of samples collected at the Royal Liverpool University Hospital, as measured by Myriad RBM's Human Oncology MAP®. Samples were obtained from individuals with PDAC with or without obstructive jaundice (PDAC high bilirubin and PDAC low bilirubin, n=15 and n=20 respectively), as well as healthy individuals (n=15) and individuals with benign biliary obstruction (n=10) and CP (n=15). *P*-values determined by Mann-Whitney U test. **(B)** Serum levels of TNC in independent samples from individuals with PDAC and high bilirubin (n=35), PDAC and low bilirubin (n=30), benign biliary obstruction (n=27) and CP (n=35), as well as healthy individuals (n=28), as measured by ELISA. *P*-values determined by Mann-Whitney U test. **(C)** TNC mRNA array expression measured as Robust Multi-array Average (RMA) in discovery fibroblast isolates (PDAC n=6, CP n=5). **(D)** qRT-PCR analysis of TNC expression in discovery and independent PDAC- (n=15) and CP-associated (n=8) fibroblasts. Expression was normalized to GAPDH using CP-associated fibroblasts as control. *P*-value determined by Mann–Whitney U test. **(E)** Representative image of TNC protein immunostaining in PDAC and CP. Scale bar=100µm (low magnification, left image; high magnification of dashed line, right image). **(F)** Proportion of PDAC (n=53) and CP (n=36) patients with TNC protein expression in the fibrotic stroma, as measured on a tissue microarray. *P*-value determined by chi-squared test. **(G)** Example of color deconvolution of α-SMA- and Masson's trichrome-stained PDAC tissue for calculation of activated stroma index (ASI). Scale bar=100µm. **(H)** ASI in PDAC cases (n=24) in **G** classified by TNC stromal protein expression. *P*-value determined by Mann–Whitney U test. **(I)** Representative image of TNC mRNA expression in PDAC stroma as determined by RNA *in situ* hybridization. Scale bar=25µm. **(J)** Proportion of PDAC (n=79) and CP (n=36) patients with TNC RNA expression in the fibrotic stroma, as measured on a tissue microarray. P-value determined by chi-squared test.

Figure 5. TNC gene silencing in PDAC-associated fibroblasts leads to a diminished TGFβ1 expression and promotes migration of pancreatic cancer cells. **(A and B)** Experimental design detailing the collection of conditioned media from PDAC-associated fibroblasts and normal activated (NA) fibroblasts **(A)** to study the functional significance of stromal TNC on MIA PaCa-2 cells using a transwell cell migration assay **(B)**. The images depict representative photographs of transwell migration assays conducted on MIA PaCa-2 cells with conditioned media from PDAC-associated fibroblasts treated with non-targeting control siRNA and two different siRNAs targeting TNC (n=7). Cell migration was quantified using QuPath. CM=conditioned media **(C)** Representative immunoblot analysis after TNC knockdown in PDAC-associated fibroblasts and normal activated fibroblasts to confirm effective knockdown before cell migration or proliferation experiments were conducted. β-actin was used as a loading control. **(D and E)** Cell migration **(D)** and proliferation **(E)** of MIA PaCa-2 cells following treatment with conditioned media from normal activated and PDAC-associated

fibroblasts with siRNA-depleted TNC. Data are expressed as mean percentage of migration or proliferation relative to control ±SEM; for the migration assays PDAC=7 and NA=6 independent experiments were performed and for proliferation PDAC=4 and NA=2 independent experiments were completed. *P*-value determined by t-test assuming unequal variance. **(F and G)** Representative immunoblot analysis of TGFβ1 after TNC knockdown in PDAC-associated fibroblasts **(F)** and normal activated fibroblasts **(G).** Densitometry quantification of TGFβ1 normalized to β-actin is shown for each fibroblast type analyzed (n=2). *P*-value determined by Student's t-test

Figure 6. TNC is modulated by mir-137 and TGFβ1 in pancreatic fibroblasts. **(A and B)** Gene array expression data of hsa-miR-212-3p and hsa-miR-137 generated using Robust Multi-array Average (RMA) from discovery fibroblast isolates (PDAC=6, CP=5). Data are shown as mean ±SEM. **(C)** Potential binding sites (bases in bold) of hsa-miR-212-3p and hsa-miR-137 predicted in the 3'UTR of TNC mRNA, alongside their mirSVR score. The more negative the score, the greater the predicted effect on mRNA. Lines represent complementary base pairing, while the grey shading depicts the seed sequence of the miRNAs shown. **(D)** qRT-PCR analysis of TNC expression in immortalized PDAC-associated fibroblasts transfected with miR-212-3p mimics (30nM), miR-137 mimics (30nM) or off-target mimics (30nM) for 48hours, plus untreated cells. Expression was normalized to GAPDH using off-target siRNA as control. Data are shown as mean ±SEM; n=2 independent experiments; *P*-value determined by paired t-test. **(E)** Western blot of TNC in resin-concentrated conditioned media and cell lysates from experiment shown in **D**. **(F)** Normalized luciferase activity of TNC 3'-UTR cloned into pGL3-Control vector containing either wild-type (WT) or mutant (MUT) binding sites of hsa-miR-137 (Supplementary Figure 2G), after co-transfection with miR-137 mimics and off-target negative control in HeLa cells. Data are fold changes of Firefly pGL3-Control constructs/Renilla pRL-SV40 vector activity ratio normalized to off-target control ±SEM; n=2 independent experiments; *P*-value determined by paired t-test. **(G and H)** qRT-PCR for TNC **(G)** and mir-137 **(H)** after incubation of PDAC-associated and normal activated (NA) fibroblasts with recombinant human TGFβ1 for 48 hours. Expression levels were compared to control (DMEM) and normalized to GAPDH and RNU6-2 respectively. Error bars depict mean ± SEM; n=3 independent experiments. P-value determined by t-test assuming unequal variance.

Figure 1

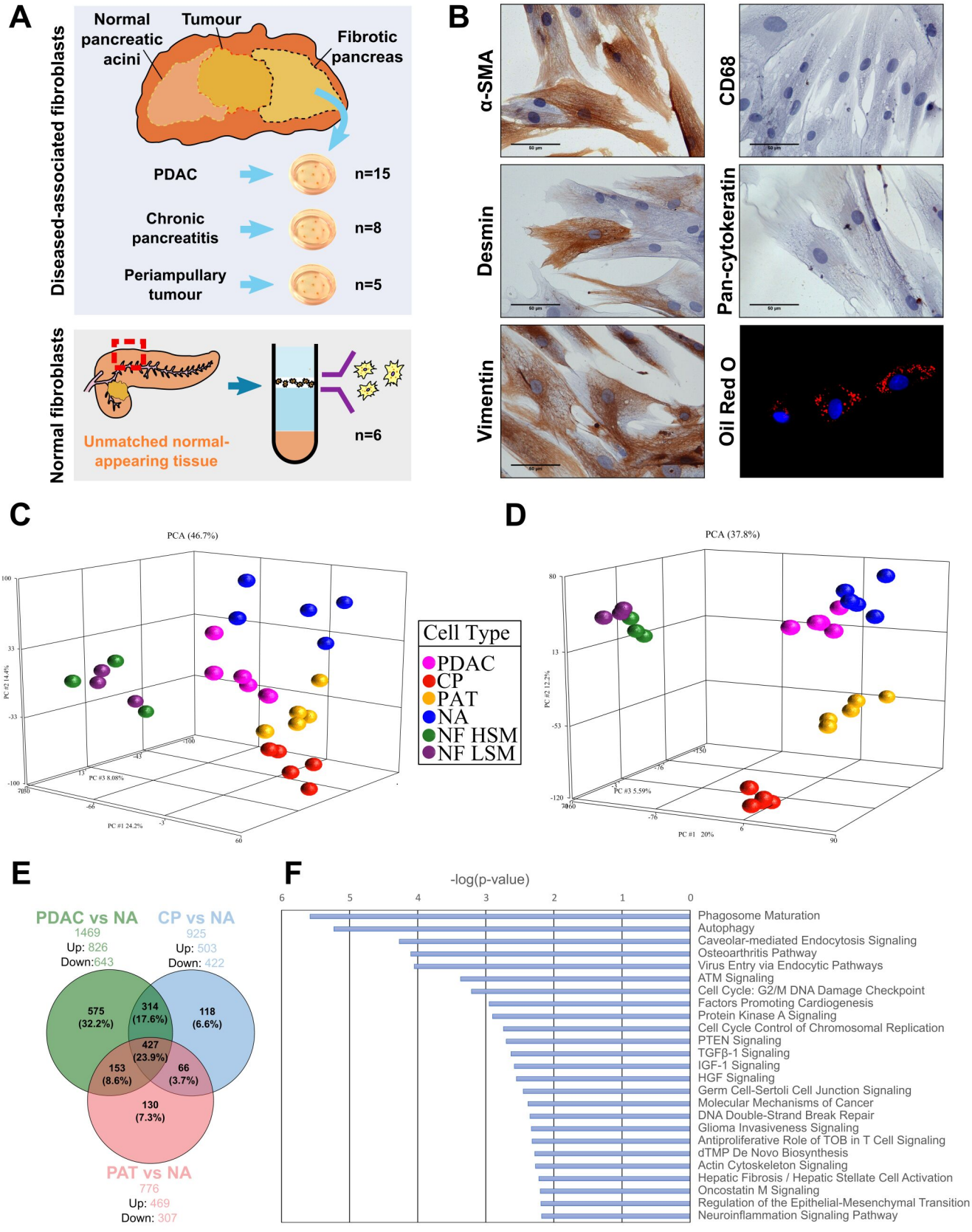
A
Diseased-associated fibroblasts
Normal pancreatic acini
Tumour
Fibrotic pancreas
PDAC
n=15
Chronic pancreatitis
n=8
Periampullary tumour
n=5
Normal fibroblasts
Unmatched normal-appearing tissue
n=6
B
α-SMA
CD68
Desmin
Pan-cytokeratin
Vimentin
Oil Red O
C
PCA (46.7%)
PC #2 14.4%
PC #3 8.08%
PC #1 24.2%
Cell Type
PDAC
CP
PAT
NA
NF HSM
NF LSM
D
PCA (37.8%)
PC #2 12.2%
PC #3 5.59%
PC #1 20%
E
PDAC vs NA
1469
Up: 826
Down:643
CP vs NA
925
Up: 503
Down: 422
PAT vs NA
776
Up: 469
Down: 307
575 (32.2%)
314 (17.6%)
118 (6.6%)
427 (23.9%)
153 (8.6%)
66 (3.7%)
130 (7.3%)
F
-log(p-value)
6
5
4
3
2
1
0
Phagosome Maturation
Autophagy
Caveolar-mediated Endocytosis Signaling
Osteoarthritis Pathway
Virus Entry via Endocytic Pathways
ATM Signaling
Cell Cycle: G2/M DNA Damage Checkpoint
Factors Promoting Cardiogenesis
Protein Kinase A Signaling
Cell Cycle Control of Chromosomal Replication
PTEN Signaling
TGFβ-1 Signaling
IGF-1 Signaling
HGF Signaling
Germ Cell-Sertoli Cell Junction Signaling
Molecular Mechanisms of Cancer
DNA Double-Strand Break Repair
Glioma Invasiveness Signaling
Antiproliferative Role of TOB in T Cell Signaling
dTMP De Novo Biosynthesis
Actin Cytoskeleton Signaling
Hepatic Fibrosis / Hepatic Stellate Cell Activation
Oncostatin M Signaling
Regulation of the Epithelial-Mesenchymal Transition
Neuroinflammation Signaling Pathway

Figure 2

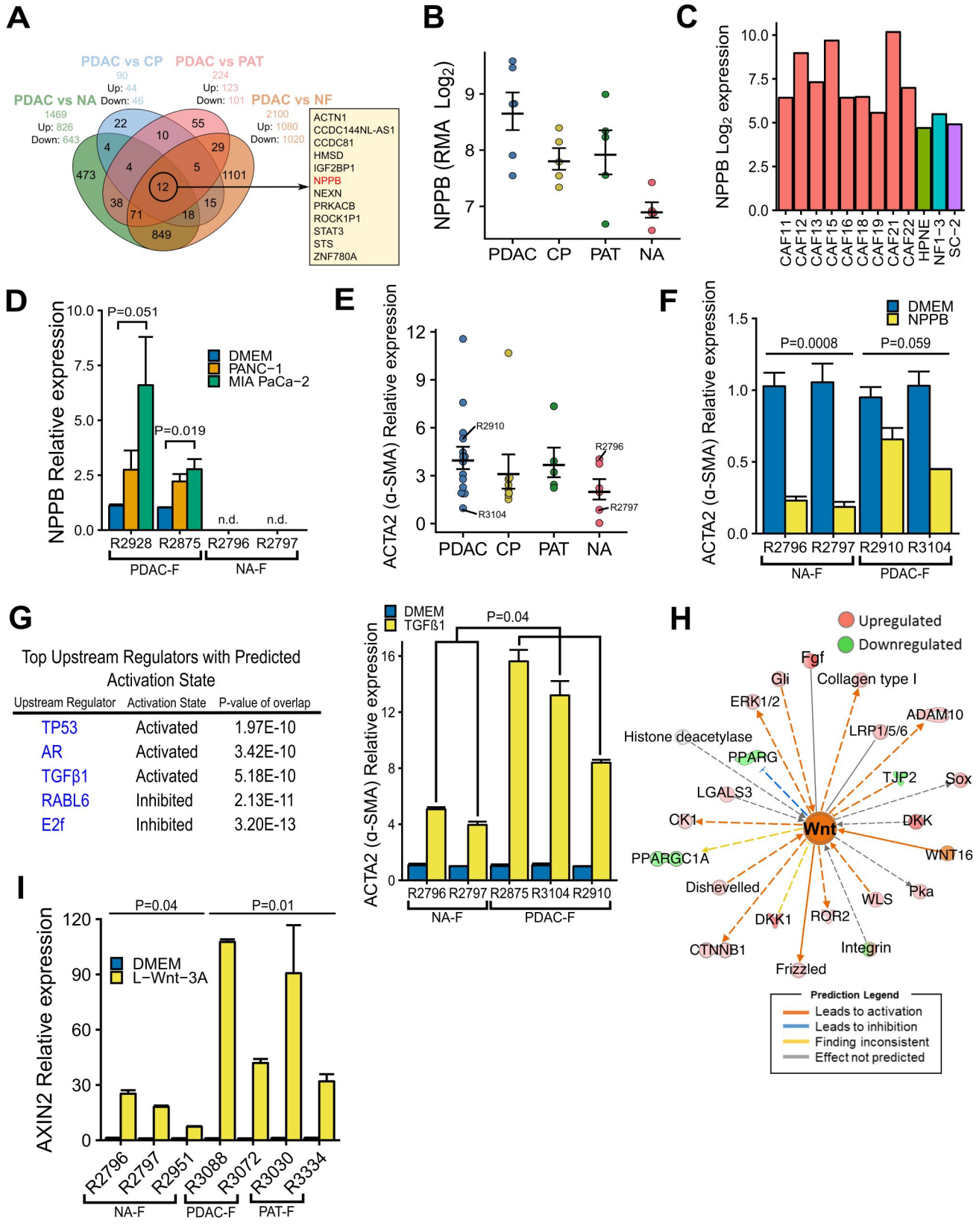
A
PDAC vs CP
90
Up: 44
Down: 46
PDAC vs PAT
224
Up: 123
Down: 101
PDAC vs NA
1469
Up: 826
Down: 643
PDAC vs NF
2100
Up: 1080
Down: 1020
22
10
55
4
29
4
5
473
1101
12
38
15
71
18
849
ACTN1
CCDC144NL-AS1
CCDC81
HMSD
IGF2BP1
NPPB
NEXN
PRKACB
ROCK1P1
STAT3
STS
ZNF780A
B
NPPB (RMA Log2)
PDAC
CP
PAT
NA
C
NPPB Log2 expression
CAF11
CAF12
CAF13
CAF15
CAF16
CAF18
CAF19
CAF21
CAF22
HPNE
NF1-3
SC-2
D
NPPB Relative expression
P=0.051
P=0.019
DMEM
PANC-1
MIA PaCa-2
n.d.
n.d.
R2928
R2875
R2796
R2797
PDAC-F
NA-F
E
ACTA2 (α-SMA) Relative expression
R2910
R2796
R3104
R2797
PDAC
CP
PAT
NA
F
ACTA2 (α-SMA) Relative expression
DMEM
NPPB
P=0.0008
P=0.059
R2796
R2797
R2910
R3104
NA-F
PDAC-F
G
Top Upstream Regulators with Predicted Activation State
Upstream Regulator | Activation State | P-value of overlap
TP53 | Activated | 1.97E-10
AR | Activated | 3.42E-10
TGFβ1 | Activated | 5.18E-10
RABL6 | Inhibited | 2.13E-11
E2f | Inhibited | 3.20E-13
DMEM
TGFß1
P=0.04
ACTA2 (α-SMA) Relative expression
R2796
R2797
R2875
R3104
R2910
NA-F
PDAC-F
H
Upregulated
Downregulated
Fgf
Gli
Collagen type I
ERK1/2
ADAM10
LRP1/5/6
Histone deacetylase
PPARG
TJP2
Sox
LGALS3
CK1
Wnt
DKK
WNT16
PPARGC1A
Dishevelled
Pka
WLS
DKK1
ROR2
CTNNB1
Integrin
Frizzled
Prediction Legend
Leads to activation
Leads to inhibition
Finding inconsistent
Effect not predicted
I
AXIN2 Relative expression
P=0.04
P=0.01
DMEM
L-Wnt-3A
R2796
R2797
R2951
R3088
R3072
R3030
R3334
NA-F
PDAC-F
PAT-F

Figure 3

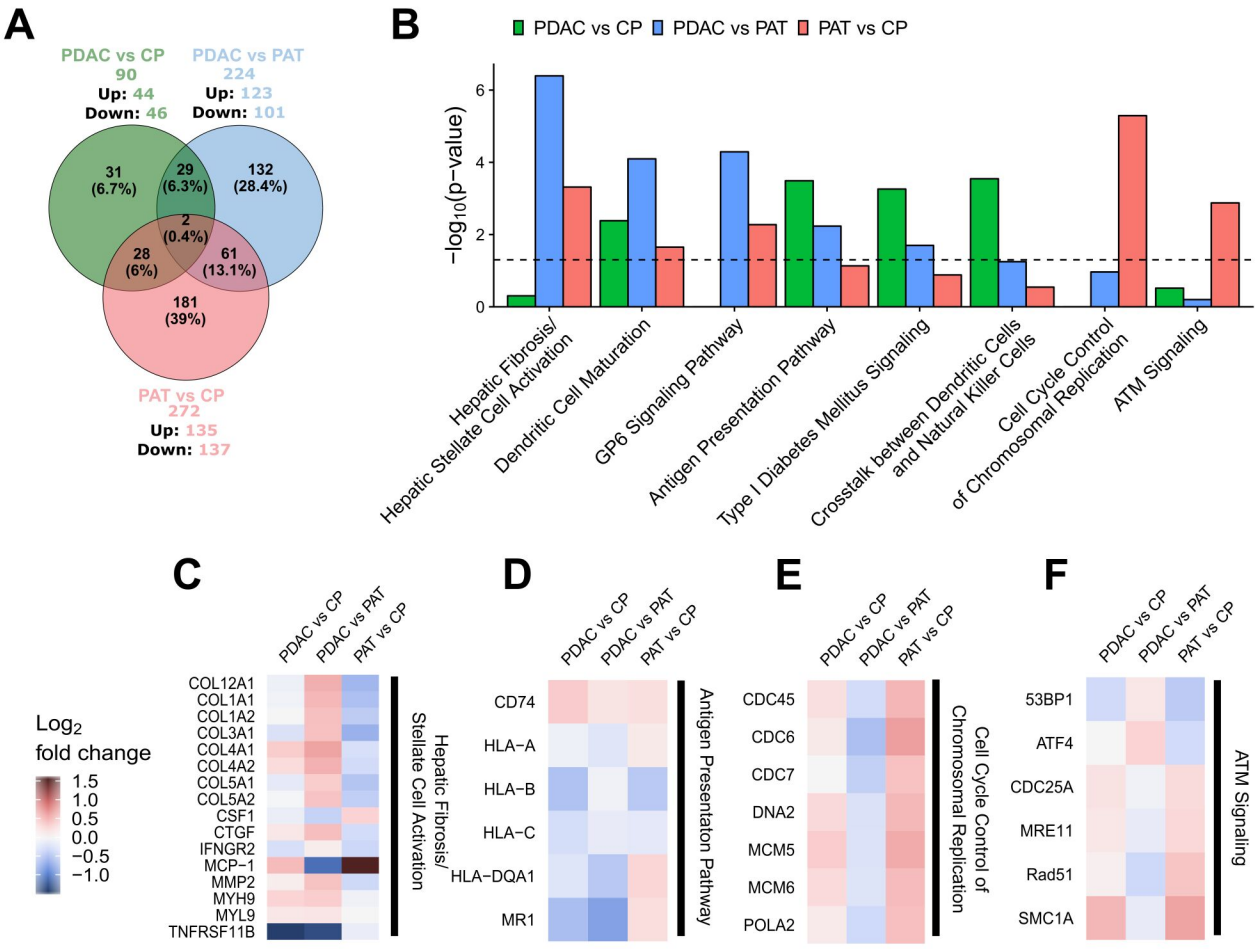
A
PDAC vs CP
90
Up: 44
Down: 46
PDAC vs PAT
224
Up: 123
Down: 101
PAT vs CP
272
Up: 135
Down: 137
31 (6.7%)
29 (6.3%)
132 (28.4%)
2 (0.4%)
28 (6%)
61 (13.1%)
181 (39%)
B
PDAC vs CP
PDAC vs PAT
PAT vs CP
−log10(p−value)
Hepatic Fibrosis/ Hepatic Stellate Cell Activation
Dendritic Cell Maturation
GP6 Signaling Pathway
Antigen Presentation Pathway
Type I Diabetes Mellitus Signaling
Crosstalk between Dendritic Cells and Natural Killer Cells
Cell Cycle Control of Chromosomal Replication
ATM Signaling
C
D
E
F
Log2 fold change
1.5
1.0
0.5
0.0
−0.5
−1.0
COL12A1
COL1A1
COL1A2
COL3A1
COL4A1
COL4A2
COL5A1
COL5A2
CSF1
CTGF
IFNGR2
MCP−1
MMP2
MYH9
MYL9
TNFRSF11B
Hepatic Fibrosis/ Stellate Cell Activation
CD74
HLA−A
HLA−B
HLA−C
HLA−DQA1
MR1
Antigen Presentaton Pathway
CDC45
CDC6
CDC7
DNA2
MCM5
MCM6
POLA2
Cell Cycle Control of Chromosomal Replication
53BP1
ATF4
CDC25A
MRE11
Rad51
SMC1A
ATM Signaling

Figure 4

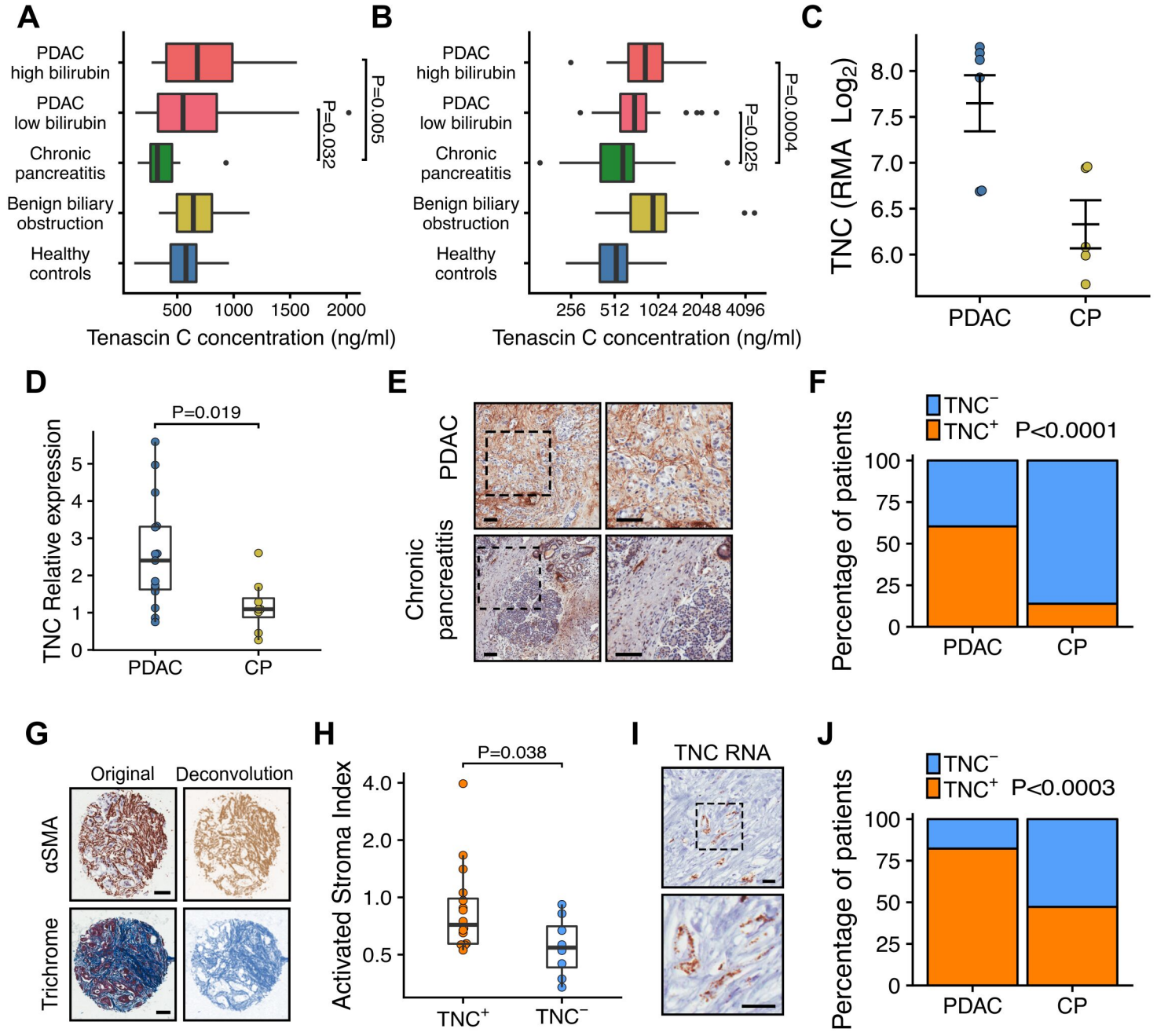
A
PDAC high bilirubin
PDAC low bilirubin
Chronic pancreatitis
Benign biliary obstruction
Healthy controls
P=0.005
P=0.032
500 1000 1500 2000
Tenascin C concentration (ng/ml)
B
PDAC high bilirubin
PDAC low bilirubin
Chronic pancreatitis
Benign biliary obstruction
Healthy controls
P=0.0004
P=0.025
256 512 1024 2048 4096
Tenascin C concentration (ng/ml)
C
TNC (RMA Log2)
8.0
7.5
7.0
6.5
6.0
PDAC
CP
D
TNC Relative expression
P=0.019
0 1 2 3 4 5
PDAC
CP
E
PDAC
Chronic pancreatitis
F
TNC⁻
TNC⁺ P<0.0001
Percentage of patients
100 75 50 25 0
PDAC
CP
G
Original
Deconvolution
αSMA
Trichrome
H
P=0.038
Activated Stroma Index
4.0 2.0 1.0 0.5
TNC⁺
TNC⁻
I
TNC RNA
J
TNC⁻
TNC⁺ P<0.0003
Percentage of patients
100 75 50 25 0
PDAC
CP

Figure 5

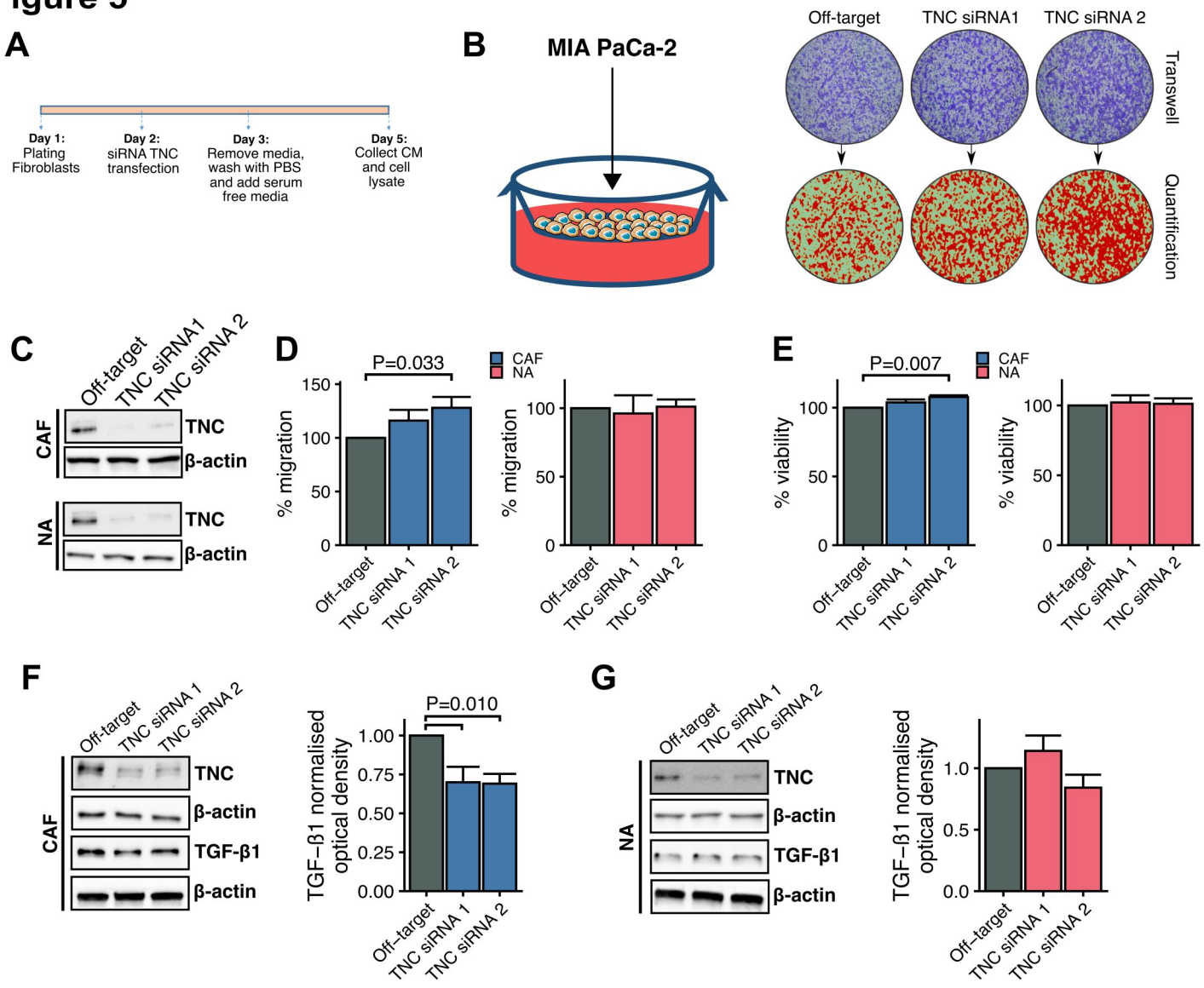
A
Day 1: Plating Fibroblasts
Day 2: siRNA TNC transfection
Day 3: Remove media, wash with PBS and add serum free media
Day 5: Collect CM and cell lysate
B
MIA PaCa-2
Off-target
TNC siRNA1
TNC siRNA 2
Transwell
Quantification
C
Off-target
TNC siRNA1
TNC siRNA 2
CAF
NA
TNC
β-actin
D
P=0.033
CAF
NA
% migration
Off-target
TNC siRNA 1
TNC siRNA 2
E
P=0.007
% viability
F
TNC
β-actin
TGF-β1
P=0.010
TGF-β1 normalised optical density
G

Figure 6

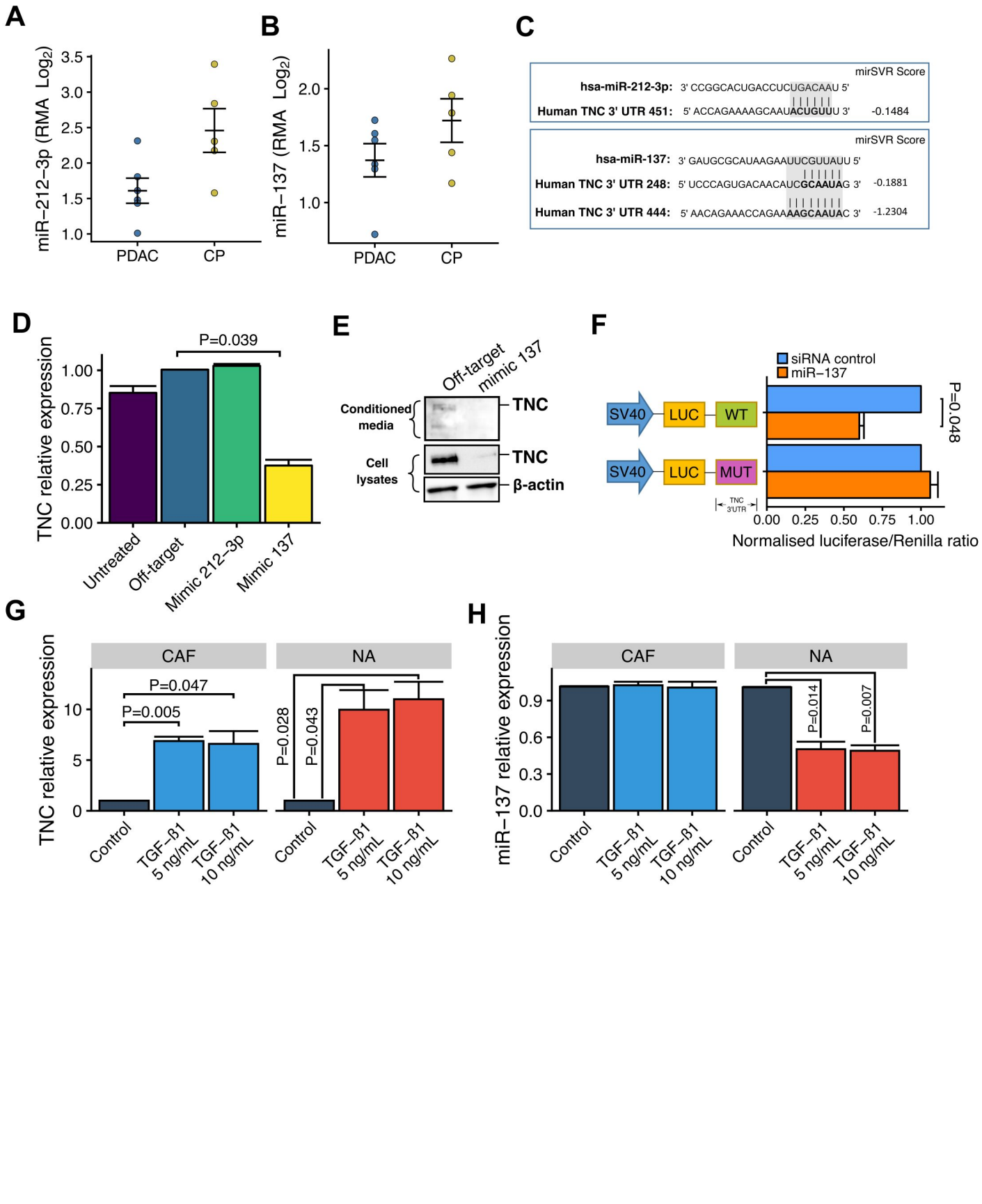
A
miR−212−3p (RMA Log2)
PDAC
CP
B
miR−137 (RMA Log2)
PDAC
CP
C
mirSVR Score
hsa-miR-212-3p: 3' CCGGCACUGACCUCUGACAAU 5'
Human TNC 3' UTR 451: 5' ACCAGAAAAGCAAUACUGUUU 3' -0.1484
mirSVR Score
hsa-miR-137: 3' GAUGCGCAUAAGAAUUCGUUAUU 5'
Human TNC 3' UTR 248: 5' UCCCAGUGACAACAUCGCAAUAG 3' -0.1881
Human TNC 3' UTR 444: 5' AACAGAAACCAGAAAAGCAAUAC 3' -1.2304
D
TNC relative expression
P=0.039
Untreated
Off-target
Mimic 212−3p
Mimic 137
E
Off-target
mimic 137
Conditioned media
TNC
Cell lysates
TNC
β-actin
F
siRNA control
miR−137
SV40
LUC
WT
SV40
LUC
MUT
TNC 3'UTR
P=0.048
Normalised luciferase/Renilla ratio
G
CAF
NA
TNC relative expression
P=0.047
P=0.005
P=0.028
P=0.043
Control
TGF−β1 5 ng/mL
TGF−β1 10 ng/mL
H
CAF
NA
miR−137 relative expression
P=0.014
P=0.007
Control
TGF−β1 5 ng/mL
TGF−β1 10 ng/mL

Supplementary Figure 1

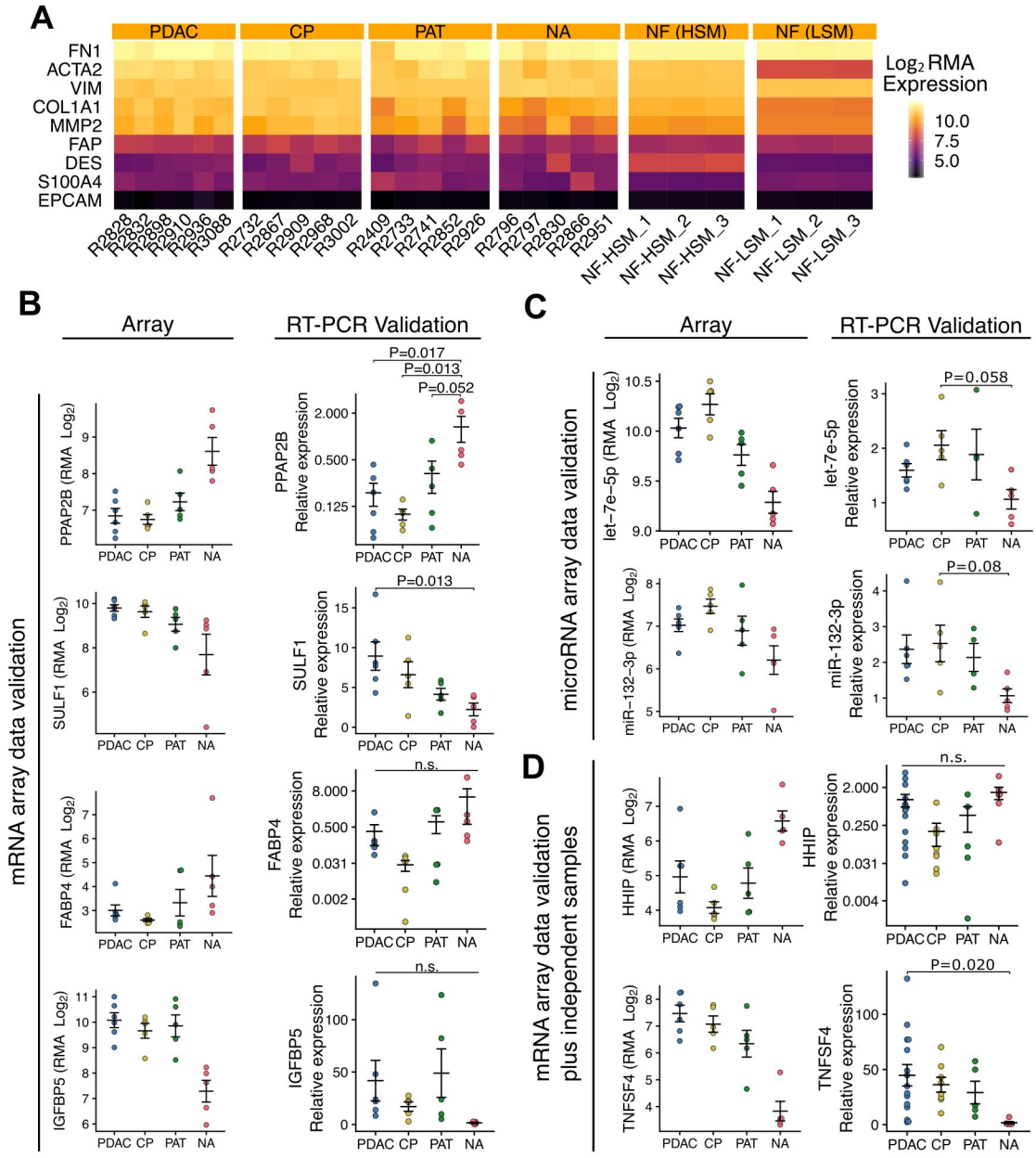

Supplementary Figure 1. (A) Heatmap representing selected genes commonly used to characterise fibroblasts. Data is taken from mRNA array expression analysis of discovery fibroblasts isolated from PDAC (n=6), CP (n=5), PAT (n=5) and primary normal PSC culture-activated (NA=5) and commercially available normal fibroblasts (NF) grown in high (NF-HSM) or low serum (NF-LSM) in triplicates each and expressed as Log2 Robust Multi-array Average (RMA). **(B and C)** Gene (mRNA **(B)** and microRNA **(C)**) array expression data of selected genes found to be significantly differentially expressed in at least one contrast within a linear model of gene expression over all the genes measured in PDAC vs NA (FDR 5%; fold change>1). Data were generated using Robust Multi-array Average (RMA) from discovery fibroblast isolates (PDAC=6, CP=5 and PAT=5) and normal PSC culture-activated (NA=5) (left panel) with validation in the same samples by quantitative RT-PCR (right panel). Patient sample analyses were performed in triplicate and the relative abundance of target genes was calculated using the delta-delta CT method. Unless otherwise stated all gene (mRNA) samples were normalized to the housekeeping gene RPLP0 and miRNA genes normalized to RNU6-2. Data are shown as mean ± SEM. P values are from an ANOVA test with a posthoc Tukey test applied for each comparison group (n.s.= not significant). **(D)** As for B with the exception that independent fibroblast isolates (PDAC=9, CP=3 and NA=1) were included in the RT-PCR validation.

Supplementary Figure 2

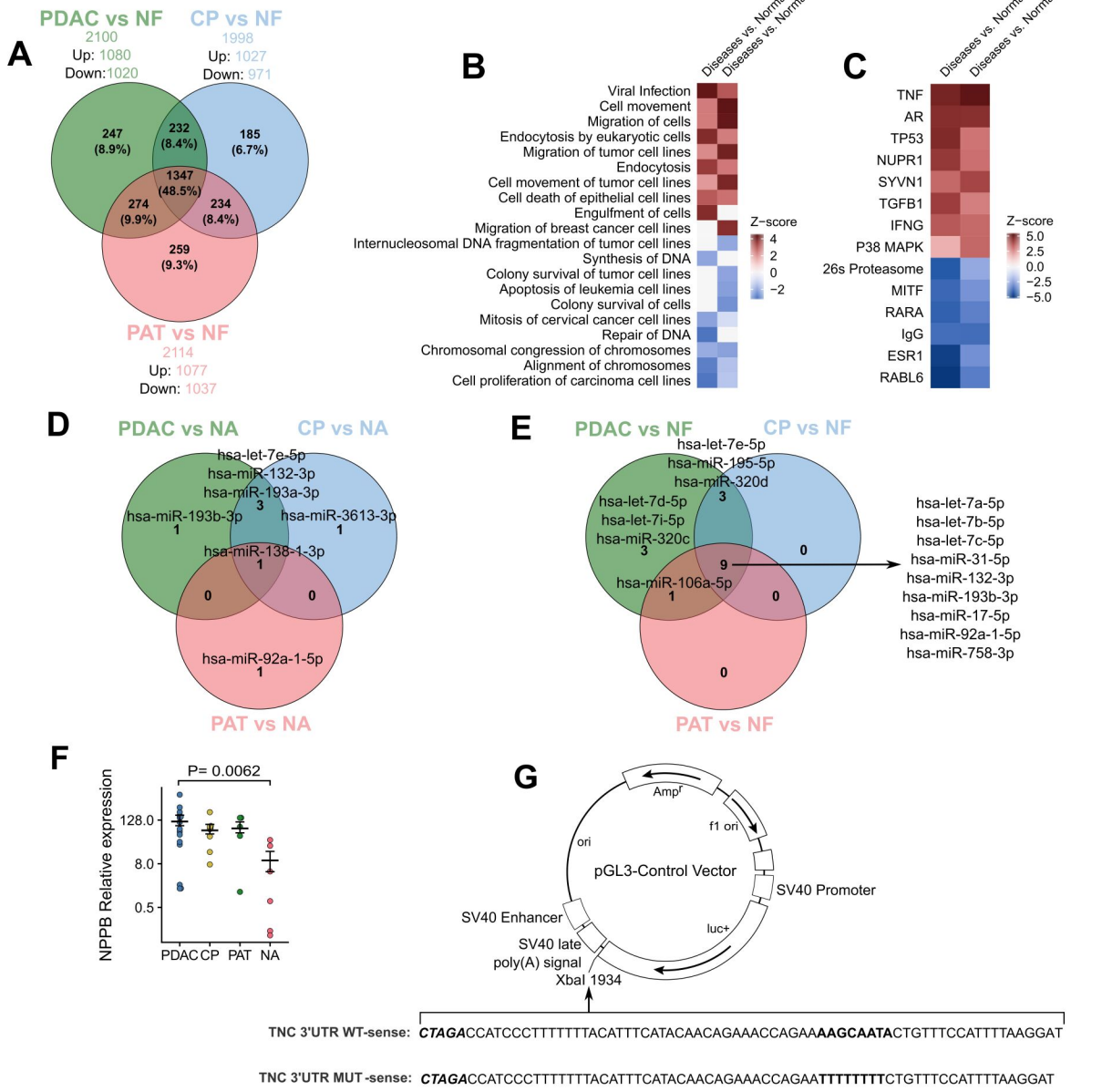

Supplementary Figure 2. **(A)** Venn diagram depicting the comparison and overlap of differentially expressed genes (mRNA array) between disease-associated fibroblasts from PDAC, CP and PAT versus NF fibroblasts, including the number of genes up- or down-regulated per contrast (the percentage is indicated in parenthesis). **(B-C)** Ingenuity pathway analysis of differentially regulated genes in disease-associated fibroblasts from PDAC, CP and PAT versus NA or NF fibroblasts showing selected top cellular and biological functions **(B)** and top upstream regulators **(C)** that are expected to be increased (positive z-score) or decreased (negative z-score) according to the IPA z-score algorithm. **(D-E)** Venn diagram depicting the comparison and overlap of differentially expressed genes (microRNA array) between disease-associated fibroblasts from PDAC, CP and PAT versus NA **(D)** or NF **(E)** fibroblasts. **(F)** qRT-PCR analysis of NPPB expression levels in discovery and independent samples of fibroblast isolates from pancreatic diseases (PDAC=15, CP=8 and PAT=5) and primary normal PSC culture-activated (NA=6). Data are shown as mean ± SEM. The P value is from a Mann-Whitney U test. **(G)** pGL3-Control Vector (copyright image Promega UK 2018) having either wild-type or mutant binding site of miR-137 in 3'UTR of TNC mRNA. The wild-type (WT) or mutated (MUT) sense sequences corresponding to a 66-bp fragment from the 3'UTR of TNC mRNA (position 7437-7502, NM_002160.3) are depicted above. The XbaI sites are indicated in bold italic and the seed region of the hsa-miR-137 targeting site are indicated in bold. The mutant was created by replacing the seed regions of the hsa-miR-137 targeting site with T (bases in bold).

Supplementary Table 1. Patient characteristics of samples used for discovery and independent validation.

	Discovery Set				Independent set		
	PDAC	CP	PAT	NA	PDAC	CP	NA
	n=6	n=5	n=5	n=5	n=9	n=3	n=1
Diagnosis for NA							
Mucinous Cystic Neoplasm				1			0
IPMN				1			0
PDAC				1			0
CP				0			0
PAT				2			1
Median age (IQR)[1]	73 (71.25-77)	46 (35-54)	67 (65-73)	64 (64-65)	65 (61-73)	37 (34.5-40)	54
Gender							
Female	5	4	5	2	4	2	1
Male	1	1	0	3	5	1	0
Stage							
IIA	1	---	0	1	1	---	0
IIB	5	---	1	0	8	---	0
III	0	---	4	2	0	---	1
Tumour differentiation							
Well differentiated	0	0	0	0	0	0	0
Moderate	2	0	1	3	2	0	0
Poor	4	0	4	0	7	0	0
Alcohol							
Yes	3	2	2	4	4	0	0
No	3	0	2	1	5	2	0
Ex	0	3	1	0	0	1	1
Smoking							
Yes	0	3	1	0	2	2	1
No	6	1	4	2	5	1	0
Ex	0	1	0	3	1	0	0
Missing	0	0	0	0	1	0	0
Diabetes							
Yes	1	2	2	1	4	1	1
No	5	2	3	4	5	2	0
Missing	0	1	0	0	0	0	0
BMI Median (IQR)	27.71 (27.01-29.25)	27.44 (27.22 – 27.66)	28.72 (26.43-29.98)	26.86 (25.27-32.84)	23.73 (21.74-25.82)	25 (23.95-25.67)	31.24
CA19-9 Median (IQR)	675 (398.25-1356)	10 (7-13)	36 (5.5-65.75)	7 (7-12)	406 (182-767)	9 (7.5-32)	---
Lymph node ratio Median (IQR)	0.117 (0.093-0.166)	---	0.5 (0.5-0.56)	0 (0-0.052)	0.181 (0.076-0.235)	---	0.75
Tumour size Median (IQR)	30 (25-40)	---	40 (25-40)	47.5 (37.5-55)	35 (28.75-41.25)	---	40

[1]IQR= interquartile range

Supplementary Table 2. Top 4 upstream regulators (with their activation z-score) significantly enriched in PDAC vs PAT and PAT vs CP, as determined using IPA.

Upstream Regulators	PDAC vs CP	PDAC vs PAT	PAT vs CP
MAPK1	2	2.21	0.74
TGFβ1	N/A	2.57	-1.19
P38 MAPK	N/A	2.21	-0.39
HIF1A	N/A	1.97	N/A

Supplementary Table 3. Patient characteristics of UoL serum sample cohorts.

	Discovery cohort					**Validation cohort**				
	PDAC non-obs[1]	PDAC-obs[2]	BBO[3]	CP[4]	HC[5]	PDAC non-obs[1]	PDAC-obs[2]	BBO[3]	CP[4]	HC[5]
n	20	15	10	15	15	30	35	27	35	28
Median age (range)	66 (39-78)	66 (39-78)	65.5 (24-80)	48 (36-78)	35 (23-65)	69 (51-83)	65 (45-81)	72 (23-86)	54 (24-78)	44 (22-77)
Sex										
F	9	8	3	9	5	17	18	12	11	20
M	11	7	7	6	10	13	17	15	24	8

[1]Pancreatic ductal adenocarcinoma without obstructive jaundice
[2]Pancreatic ductal adenocarcinoma with obstructive jaundice
[3]Benign biliary obstruction
[4]Chronic pancreatitis
[5]Healthy control

Supplementary Table 4. Patient characteristics of samples included on TMAs histologically stained for TNC.

	PDAC[1] TMA #1	PDAC[1] TMA #2	CP[2] TMA
n	41	48	47
Median age (range)	67 (45-81)	68 (44-84)	52 (21-77)
Sex			
F	21	23	25
M	20	25	21
Missing	0	0	1

[1]Pancreatic ductal adenocarcinoma
[2]Chronic pancreatitis

Supplementary Material and Methods

Immunocytochemistry

Cells were seeded on coverslips and fixed in 10% formalin (Sigma), permeabilized using 0.5% Triton X-100 for 10min and blocked for endogenous peroxidases using 1% hydrogen peroxide in methanol. Cells were washed 3 times with TBS before the addition of blocking solution (TBS containing 10% goat serum and 1% bovine serum albumin) for 30min at room temperature after which primary antibodies: anti-aSMA (1:500, Abcam #ab7817), anti-vimentin (1:1000, Abcam #ab8978), anti-desmin (1:500, Abcam #ab15200), anti-pan-cytokeratin (1:300, Abcam #ab9377) and anti-CD68 (1:500, Santa Cruz #sc-9139) were diluted in blocking solution and added to the cells for overnight incubation at 4˚C. Cells were washed and incubated with either horseradish peroxidase (HRP)-conjugated secondary goat-anti-rabbit (1:100, Dako #P0448) or goat-anti-mouse (1:200, Dako #P0447) for 30min at room temperature and washed. A matching isotype control was included in each staining experiment. Color was developed using the DAB chromogen system (Dako) for 5 min. Cells were counterstained with Mayer's hematoxylin (Sigma) for 5 minutes.

RNA isolation

Total RNA (containing small RNAs) was isolated using the high pure miRNA isolation kit (one-column protocol) (Qiagen) following the manufacturer's instructions. Purified total RNA was cleaned from genomic DNA using the DNA-freeTM DNA removal kit (ThermoFisher Scientific) following the manufacturer's instruction. The median RNA integrity number (RIN) for the discovery samples applied to the mRNA/miRNA array was 8.1 (IQR= 7.7-8.4) (Agilent 2100 Bioanalyser). Quality and quantity of total RNA was assessed by NanoDropTM 2000C (ThermoFisher Scientific).

Array Data Analysis

Probe expression data for mRNA and miRNA was generated from CEL files using Robust Multi-Array Average (RMA) normalization in Partek Genomics Suite software. Data were analyzed in R/Bioconductor with appropriate Affymetrix annotation.

Differential expression analysis

After normalization, mRNA probe measurements corresponding to 70,524 Affymetrix probe sets were mapped to 25,195 HUGO gene symbols per array. Measurements from 36,353 miRNA probe sets (representing 208 different species) included 6,631 human probe sets per array. Measurements from all probe sets were used for effective normalization while human only probe sets were used for miRNA expression analysis.

Differential expression analysis of both mRNA and miRNA was performed using the Biocondcutor package limma. A design matrix was constructed with CP, PDAC, PAT, NA, NF-HSM, NF-LSM, RNA labelling date, array scan date and culture time as factors. The first six factors were biological factors representing fibroblast cell lines (from diseased tissue, normal adjacent tissue and commercial sources). While RNA labelling and scan dates were included to remove the influence of batch processing, culture time was included as an ordinal factor indicating relative duration of cell culture prior to nucleic acid extraction (≤7 days in culture=1; 8 to 14 days in culture =2; ≥15 days in culture=3). A linear model was fitted using this design before contrasts were generated in a second linear model for inference of differential expression. Contrasts were generated to compare cell-wise comparisons PDAC vs. CP; PDAC vs. PAT; PDAC vs. NA; PDAC vs. NF-HSM; CP vs. NA; CP vs. NF-HSM; PAT vs. NF-HSM; PAT vs. NA; PAT vs. CP; NF-HSM vs. NF-LSM; NA vs. NF-LSM; NA vs. NF-HSM. A further disease-wise set of contrasts was generated by pooling all diseased fibroblasts (PDAC, CP and

PAT) and comparing this group to NA and NF, respectively. The nestedF multiple testing strategy from the decideTests function in limma with FDR cut off 5% was used to avoid the accumulation of probe-wise and contrast-wise false positives. Clustering of expression data was performed in Partek Genomics Suite. For heat maps, samples and probes were clustered by average linkage using Euclidean distance.

Pathway analysis of differentially expressed genes

Using Ingenuity Pathway Analysis (IPA) core analysis was performed for functional analysis of differentially enriched gene lists. Canonical pathways were considered statistically significant if the negative log likelihood enrichment score exceeded 1.3. IPA upstream regulator function was used to determine potential transcriptional regulators to explain the identified changes in gene expression between the different fibroblasts comparison groups. The activation z-score was used to predict activation or inhibition of canonical pathways and/or transcriptional regulators based on published findings curated in IPA.

Gene expression omnibus deposition

The data discussed in this publication have been deposited in NCBI's Gene Expression Omnibus and are accessible through GEO Series accession number GSE123378 (https://www.ncbi.nlm.nih.gov/geo/query/acc.cgi?acc=GSE123378).

Quantitative real-time PCR Analysis for mRNA and microRNA

Total RNA obtained from fibroblasts was reverse transcribed to form cDNA using the QuantiTect RT Kit (Qiagen) for mRNA analysis or the miScript II RT kit (Qiagen) for microRNA analysis and amplified

with a ready-to-use hot start reaction mix for SYBR Green I-based qRT-PCR (Roche) using the LightCycler® 480 Instrument. The primer sequences from PPAP2B, SULF1, FABP4, IGFBP5, HHIP, TNFSF4, TNC, ACTA2, AXIN2, RPLP0 and GAPDH were obtained from Primerdesign Ltd and primer sequences from NPPB, TGF-β1, hsa-let-7e-5p, hsa-miR-132-3p and RNU6-2 were obtained from Qiagen. mRNA or microRNA levels of the target genes analyzed were normalized with the corresponding housekeeping RNA level in the same sample. All reactions were performed in triplicate. In addition, a cDNA-free negative control and a reverse transcriptase free control was included. The results were calculated using the 2ΔCt method.

Amplification refractory mutation system (ARMS) for KRAS mutation

The KRAS mutation status of 6 specific point mutations (G12R, G12S, G12C, G12D, G12V, G12A) was evaluated as previously described (40).

Conditioned media concentration

Conditioned media was collected and centrifuged at 800g (at 4˚C) for 7min and processed with StrataClean resin (Agilent) for concentration of proteins. Briefly, a ratio of 1:400 (resin:sample) was mixed and vortexed for 1min and centrifuged at 800g (4˚C) for 1min. Supernatant was removed and resin washed twice with 500µl of 50mM ammonium bicarbonate and resuspended in 80µl of this solution. Samples were aliquoted and stored in -80˚C until use.

Protein Extraction

Cells were washed twice with cold PBS before addition of RIPA buffer supplemented with cOmplete™, Mini, EDTA-free Protease Inhibitor Cocktail (Roche) for 5 min. Cells were harvested with

a cell scrapper and transferred to a microcentrifuge tube on ice for 15 min (vortexing the samples 3 times for 1 min at full speed during incubation). Cell debris was removed by centrifugation at 14,000 × g for 15 min at 4°C, proteins were then quantified using the Bicinchoninic acid assay (ThermoFisher Scientific).

Immunoblotting of conditioned media and cell lysates.

Conditioned media from fibroblasts was collected and proteins concentrated with StrataClean resin (Agilent). Equal volumes of resin were mixed with loading buffer and heated at 95°C for 15 min and separated using SDS-PAGE before transferal to a PVDF membrane that was subsequently blocked in 5% BSA for 1 hour before overnight incubation at 4°C with a TNC antibody (Novus Biologicals, #NB110-68136) diluted 1:1000. A further incubation followed for 1 hour at room temperature, with secondary anti-mouse HRP-bound antibodies (Dako) diluted 1:3000 in 5% BSA.

For cell lysates, equivalent amounts of protein (5µg for TNC and 10µg for TGF-β1) were mixed with loading buffer and heated at 95 °C for 15 min to be size fractioned using SDS-PAGE before transfer to a PVDF membrane. The membrane was blocked in a 1% milk - 3% BSA mix for 1 hour with an overnight incubation at 4°C with the same TNC antibody (1:5000 dilution) or TGF-β1 (Abcam, # ab92486; 1:500 dilution). A further incubation followed for 1 hour at room temperature, with secondary anti-mouse or anti-rabbit HRP-bound antibodies respectively (Dako) diluted 1:5000 in a 1% Milk - 3% BSA mix. Monoclonal anti-β-actin antibody (Sigma, #A2228) was used to check for protein loading. Images were visualized using western ECL substrate (Bio Rad) in a ChemiDoc Touch Imaging System (Bio Rad).

Luciferase reporter gene construct

A 66-bp oligonucleotide fragment from the 3'-unstranslated region (3'-UTR) of TNC (position 7437 to 7502, NM_002160.3) containing the miR-137 binding sites were cloned into the XbaI site of the pGL3-Control firefly luciferase reporter vector (Promega). A mutant construct was also generated by mutating the seed region of the miR-137 binding sites. The constructs were then confirmed by sequencing. HeLa cells were co-transfected using Lipofectamine 2000 (Invitrogen) with 100ng of each reporter constructs containing either the targeting sequence of the TNC 3'-UTR or its mutant in addition to miR-137 mimics (50nM) and off-target-AllStars negative control (50nM) (Qiagen). The pRL-SV40 vector (promega) was also co-transfected using 10ng to act as a Renilla luciferase control. The luciferase activities were measured 48h after transfection using Dual-Luciferase reporter assay system (Promega) and a Varioskan Flash microplate reader (Thermo Scientific) according to manufacturer's instructions.

Normal activated and PDAC-associated fibroblast immortalization

To prepare retrovirus, packaging Phoenix cells were seeded and transfected 24h later with pWZL-Blast-Flag-HA-hTERT (Addgene) using calcium-phosphate-mediated transfection. Normal activated and PDAC-associated fibroblasts were infected with retroviruses produced in the packaging cells (24h after transfection) in the presence of 5µg/mL Polybrene (Millipore) and were selected with 5µg/mL blasticidin (Thermofisher Scientific). An additional plate of non-infected cells were included as a control to ensure drug selection.

Activated stroma index (ASI) quantification

Cores from successive PDAC TMAs stained for α-SMA and collagen were matched and quantified using ImageJ version 1.5. Color deconvolution was performed to isolate brown α-SMA staining and blue collagen staining. Images were deconvoluted into three colors using the RGB color model. The

following thresholds were used for α-SMA: Color 1 R=0.6027735, G=0.644836, B=0.46994755; Color 2 R=0.34126425, G=0.56168777, B=0.753688; Color 3 R=0.7212509, G=0.5183564, B=0.45946032. For collagen: Color 1 R=0.76523894, G=0.5705916, B=0.29805133; Color 2: R=0.5437807, G=0.6563658, B=0.52295935; Color 3 R=0.34454608, G=0.4935677, B=0.79854804.

Deconvoluted images were converted to 8-bit binary greyscale images, using the 'Triangle' auto-threshold algorithm, and scaled to enable quantification of stained area in μm^2. The activated stroma index was calculated as α-SMA area (μm^2) ÷ collagen area (μm^2) and the mean calculated across cores for each patient.

Immunohistochemistry and Masson's trichrome staining

Deparaffinization and antigen retrieval were performed using pH9 antigen retrieval buffer in a PT Link (Dako). Sections were washed in 0.1% TBS Tween® 20 and blocked for endogenous peroxidases using peroxidase blocking reagent (Dako) at room temperature for 10 minutes. After further washing sections were dried and incubated with tenascin C antibody (clone 4C8MS, Novus Biologicals) diluted 1:200 or α-SMA (Abcam) diluted 1:50 in antibody diluent (Dako) for 1 hour at room temperature. Incubation with labelled polymer anti-mouse secondary antibody (Dako) followed for a further 1 hour at room temperature prior to visualisation with DAB+ chromogen (Dako), before counterstaining with haematoxylin then dehydration and mounting. Masson's trichrome staining for collagen was performed according to the manufacturer's instructions (Sigma-Aldrich). All whole sections and TMAs were qualitatively reviewed by a specialized histopathologist (FC).

RNA in situ hybridisation

In situ hybridization was performed using a commercial assay platform with probes specific for TNC (RNAscope® Reagent Kit, Advanced Cell Diagnostics), according to the manufacturer's instructions

using the ‘Standard’ pretreatment protocol. Each run was accompanied with sections probed for peptidylprolyl isomerase B (PPIB) and dihydrodipicolinate reductase (dapB), a bacterial enzyme, as positive and negative controls for mRNA expression, respectively.